Development of a Piston Ring Pack Model for Internal Combustion Engines

Spyridon Antonopoulos

Supervisor: C.I. Papadopoulos, Assist. Prof. NTUA

Thesis Committee Members: L. Kaiktsis, Assoc. Prof. NTUA
G. Papalamprou, Assist. Prof. NTUA

School of Naval Architecture and Marine Engineering
Department of Marine Engineering
National Technical University Of Athens

a thesis submitted in partial fulfillment of the requirements for the degree of
Diploma of Naval Architecture and Marine Engineering

October 2017

Acknowledgements

First of all I would like to thank my supervisor, Assistant Professor C. Papadopoulos for the support, the guidance and the motivation he provided me with to carry out my diploma thesis. I would also like to thank my colleagues and friends, An. Charitopoulos, S. Nanopoulos and St. Siamantas, for their assistance, advice and company over the last year.

I would like to take this opportunity to thank all of my professors in the School of Naval Architecture and Marine Engineering, NTUA, that contributed to my education during my attendance as a student.

Last but not least, I would like to thank my parents for their loving support throughout my studies.

Abstract

Internal combustion engines are widely used in industry. In the maritime industry, a variety of different combustion engines are used to provide propulsion and electric power. Typically, a conventional cargo ship operates with one large bore 2-stroke marine engine that is directly coupled with the propeller to provide the required thrust, while a set of two or more smaller 4-stroke engines generate the electricity for hotel loads, machinery operation, navigation systems, etc.

Strict regulations regarding the emissions of the ships, as well as the need for the minimization of running and maintenance costs are important factors that dictate the development of technologically advanced IC engines. Moreover, reliability is critical, considering that safety at sea is of the utmost importance.

The piston ring pack assembly in IC engines plays an essential role as it provides the necessary dynamic seal for the combustion chamber. Energy losses due to friction in the ring pack account for approximately 1.1 to 4 percent of the total energy loss in the engine. Thus, design for minimization of friction in ring packs is meaningful. Furthermore, design for minimization of the blow-by increases the engine's efficiency while it reduces the unburned hydrocarbon emissions. Another important aspect of piston ring pack design is wear as ring replacement can be very expensive for large bore 2-stroke marine engines. On some occasions, extensive wear can also shorten the engine's life.

In the present study, a two-dimensional model for the simulation of the piston ring pack system has been developed. Physical formulation allows for the ring dynamics and gas dynamics to be coupled in an integrated model. This model is capable of predicting ring movement, gas pressure in both the back of the ring and the inter-ring volumes, and gas flow in the various crevices of the ring pack system.

A simplified software model has been implemented for a 4-stroke gasoline engine and has been validated against literature data. In particular, given the land pressures and the ring motion, the present model is capable of calculating the pressure distribution acting on the ring generated by three different phenomena: pressure generation due to the gas in the ring-groove channel, pressure by the oil in the piston groove, and asperity contact pressure between the ring and its groove. The implemented model is also capable of calculating the

gas flows through the ring groove channel and the ring gap. The validity of the model has been verified by comparisons with both the outputs of a similar published model and with experimental data.

Σύνοψη

Οι μηχανές εσωτερικής καύσεως χρησιμοποιούνται ευρέως στη βιομηχανία. Στη ναυπηγική, ένα πλήθος διαφορετικών μηχανών εσωτερικής καύσης χρησιμοποιούνται για την παραγωγή πρόωσης και ηλεκτρικής ενέργειας. Συνήθως, ένα συμβατικό φορτηγό πλοίο λειτουργεί με έναν μεγάλο δίχρονο κινητήρα Diesel που συνδέεται άμεσα με την έλικα μέσω ενός άξονα, ενώ δύο οι περισσότεροι μικρότεροι 4-χρονοι κινητήρες βενζίνης παράγουν την απαιτούμενη ηλεκτρική ενέργεια για τους χώρους ενδιαίτησης, τα σύστημα πλοήγησης, τα υδραυλικά συστήματα και τα λοιπά βοηθητικά μηχανήματα.

Οι αυστηροί κανόνες για τις εκπομπές ρύπων από τα πλοία, αλλά και η ανάγκη για ελαχιστοποίηση του κόστους λειτουργίας και συντήρησης, είναι σημαντικοί παράγοντες που κάνουν επιτακτική την ανάγκη για την ανάπτυξη τεχνολογικά προηγμένων κινητήρων. Επιπρόσθετα, η αξιοπιστία είναι ένας ακόμη παράγοντας υψίστης σημασίας, δεδομένης της ανάγκης για ασφάλεια στη θάλασσα.

Το σύστημα ελατηρίων εμβόλου στις μηχανές εσωτερικής καύσης έχει ως στόχο την δυναμική μόνωση του θαλάμου καύσης. Οι εκροές ενέργειας λόγω τριβών από το σύστημα ελατηρίων ευθύνεται για περίπου το 1.1 με 4.0% των συνολικών απωλειών ενέργειας στον κινητήρα. Συνεπώς, η σχεδίαση με στόχο την ελαχιστοποίηση της τριβής στο σύστημα ελατηρίων αποκτά σημασία. Επιπλέον, η σχεδίαση για την ελαχιστοποίηση εκροών καυσαερίου από τον θάλαμο καύσης αυξάνει τον βαθμό απόδοσης της μηχανής, ενώ ταυτόχρονα μειώνει τις εκπομπές άκαυστων υδρογονανθράκων. Ένας ακόμη σημαντικός παράγοντας για την σχεδίαση του συστήματος ελατηρίων είναι η φθορά, καθώς η αντικατάσταση ελατηρίων είναι ιδιαίτερα ακριβή για μεγάλους δίχρονους ναυτικούς κινητήρες Diesel, ενώ σε ορισμένες περιπτώσεις, η εκτεταμένη φθορά μπορεί να οδηγήσει σε μειωμένο χρόνο ζωής της μηχανής.

Στην παρούσα εργασία, αναπτύχθηκε ένα δισδιάστατο μοντέλο για την προσομοίωση του συστήματος ελατηρίων εμβόλου. Η φυσική διαμόρφωση του μοντέλου επιτρέπει την ζεύξη της δυναμικής των ελατηρίων με τη δυναμική του καυσαερίου στο σύστημα. Το μοντέλο αυτό είναι ικανό να προβλέψει την κίνηση των ελατηρίων, την πίεση του αερίου πίσω από το ελατήριο και στον χώρο μεταξύ δύο διαδοχικών ελατηρίων, και τη

ροή μάζας αερίου στα διάφορα κανάλια του συστήματος ελατηρίων, σε κάθε χρονική στιγμή λειτουργίας.

Το αναπτυχθέν μοντέλο εφαρμόστηκε τμηματικά σε 4-χρονο κινητήρα βενζίνης και έγινε επαλήθευση με τη βοήθεια αποτελεσμάτων της βιβλιογραφίας. Πιο αναλυτικά, το εν λόγω μοντέλο, λαμβάνοντας ως εισαγωγή την κίνηση του ελατηρίου και τις πιέσεις στους διάφορους χώρους (πίσω, πάνω, και κάτω από το ελατήριο), είναι ικανό να υπολογίζει την κατανομή πίεσης πάνω στις πλευρές του ελατηρίου λόγω των εξής τριών διαφορετικών φαινομένων: ανάπτυξη πίεσης λόγω της ύπαρξης αερίου στο κανάλι μεταξύ του ελατηρίου και της αυλάκωσης, ανάπτυξη πίεσης από το λιπαντικό φιλμ που είναι εναποτεθημένο πάνω στην αυλάκωση, και ανάπτυξη πίεσης λόγω της επαφής τραχύτητας μεταξύ της πλευράς του ελατηρίου και της αντίστοιχης πλευράς της αυλάκωσης. Το αναπτυχθέν μοντέλο είναι ικανό, επίσης, να υπολογίζει τις ροές μάζας αερίου στο κανάλι μεταξύ του ελατηρίου και της αυλάκωσης και στο άνοιγμα του ελατηρίου. Η ακρίβεια του μοντέλου επαληθεύτηκε μέσω σύγκρισης των αποτελεσμάτων του τόσο με αποτελέσματα παρόμοιου μοντέλου, όσο και με πειραματικά δεδομένα.

Contents

List of Figures

List of Tables

Nomenclature

Roman Symbols

A	asperity contact coefficient
$a_{r,0}$	static twist of the ring r
B	cylinder bore diameter
d_{CG}	distance of the ring running surface from the centre of gravity of the ring
d_r	depth of ring r
d_{ref}	normalisation value for the radial axis
$D_{r,outer}$, $D_{r,inner}$	outer and inner diameter of the ring r, respectively
E_g	elastic modulus of the groove
E_r	elastic modulus of ring r
$F_{5/2}$	Gaussian distribution of the $Z = 5/2$ score
$F_{inertia}$	inertia force due to piston acceleration
$F_{n,og}$	oil and gas force acting on the ring
F_{radial}	concentrated ring liner force at minimum point x_0
$F_{sl,u/l}$	force on the ring generated by the gas pressure between the piston skirt and the cylinder liner clearance, upper and lower
g_w	width of the groove
h_a	distance between the ring and its groove at the entrance of the channel
h_b	distance between the ring and its groove at the exit of the channel

h_{ref} normalisation value for the axial axis

h_{sl} distance between the piston skirt and the cylinder liner

I_r moment of inertia of the ring r

K and K' asperity contact coefficients

l cylinder rod length

l_1, l_2 parts of the running surface above and below the centre of gravity of the ring

$\dot{m}_{gas,i,j}$ channel gas flow between volumes i and j

$\dot{m}_{gd}$ mass flow rate of the gas in a ring groove orifice due to gas displacement

$\dot{m}_{gda}$ local mass flow rate of the gas at the entrance of the ring and groove orifice due to gas displacement

$\dot{m}_{gdb}$ local mass flow rate of the gas at the exit of the ring and groove orifice due to gas displacement

m_{gd} mass of the gas in a ring groove orifice

m_i gas mass in volume i

$M_{n,og}$ oil and gas moment acting on the ring

m_r total mass of the ring r

M_{rs} moment generated at the ring running surface of the ring

$M_{sl,u/l}$ moment on the ring generated by the gas pressure between the piston skirt and the cylinder liner clearance, upper and lower

M_{tors} moment created by the torsional deformation of the ring

o piston pin offset

p_0 normalisation value for pressure

$p_{upper}, p_{lower}, p_{back}$ gas pressure generated above and below the ring running surface and at the back of the ring, respectively

p_c average asperity contact pressure distribution when both surfaces are rough

p_i gas pressure in volume i

$p_{u/l}$ gas pressure between the piston skirt and the cylinder liner clearance, upper and lower

r engine crank radius

r_w width of the ring r

T_i gas temperature in volume i

T_r torsional stiffness of ring r

υ_g Poisson's ratio of groove

V_i geometrical volume per unit length in volume i

υ_r Poisson's ratio of ring r

W_r weight force acting on the piston ring

x, $\dot{x}$,$\ddot{x}$ piston position, velocity and acceleration

x_0 minimum ring running surface profile point

X_1, X_2 local ring flank edges at the entry and the exit of the ring groove channel

z asperity contact exponent coefficient

Greek Symbols

β radius of the curvature of the paraboloidal asperities

η surface density of asperities

γ adiabatic index

$\kappa_{fl,r}$ coefficients for the spacial terms of the gas displacement equations in flank fl and ring r

$\lambda_{fl,r}$ coefficients for the pressure variation terms of the gas displacement equations in flank fl and ring r

ω rotational speed of the crankshaft

ϕ cylinder crank angle

σ variance of the composite surface roughness

Subscripts

fl ring flank $fl = 0, 1$ for upper and lower flanks, respectively

n subscript indicating non-dimensionilised variable

r ring r

Chapter 1

Introduction

1.1 The Significance of the Piston Ring Pack

Minimization of running and maintenance costs, reliability, environmental pollution and customer satisfaction are the key factors being considered for the development of modern internal combustion engines [15]. Pollutants are being regulated by ever stricter emission standards both in the automotive [5] and the maritime [14] industries. Technology advancement of the piston, ring and liner assembly towards engine efficiency, lower pollutants emissions, minimization of engine components wear and consumption of lubricants, is led by the aforementioned requirements.

Piston ring packs for internal combustion engines have to meet a list of requirements to provide a sufficient dynamic seal for reciprocating linear motion under demanding conditions [1]:

- Low friction, for supporting a high efficiency of the engine
- Low wear of the ring, for ensuring a long operational lifetime
- Low wear of the cylinder liner, for retaining the surface texture of the liner and minimizing conformability issues
- Limit the flow of the engine oil (four-stroke engines) to the combustion chamber, for lower emissions and minimize the oil consumption in general
- Provide sufficient sealing in order to minimize blow-by
- Provide resistance against mechanical and thermal fatigue and erosion
- Provide reliable operation and cost effectiveness

According to Richardson, mechanical friction losses contribute to 4 to 15 percent of the total energy produced by an internal combustion engine, of which the piston assembly could account for 40 to 55 percent [16]. The piston ring pack contributes to 28 to 45 percent of the piston assembly mechanical friction losses, resulting in a total energy loss of 1.1 to 4.0 percent. The distribution of the ring pack friction losses is further analyzed in 50 to 75 percent of the ring pack friction being generated by the oil ring, 13 to 40 percent being generated by the top ring and 10 to 22 percent by the second ring.

Concerning the blow-by process, Zhao and Lee [22] state that, although formation of soot, NOx and other emission species occurs in the cylinder chamber in large bore diesel engines, for small bore diesel engines, the effect of fuel vapor immersing into the oil layer is significant, resulting in 42 percent of unburnt hydrocarbon emissions that are developed from the crevice flow process in the ring pack. For the estimation of the blow-by in such occasions, ring dynamics are critical [12].

Wear occurs in the cylinder system due to the asperity contact between moving parts, altering the performance and greatly affecting blow-by, friction and oil consumption in the engine [18]. Excessive wear may result in unpredictable performance and, as a result, shorten the lifetime of the engine. Understanding of the wear can be attained by modeling the asperity contact pressure distribution between the rings and the liner, as well as, between the rings and the piston grooves.

Numerical simulation can be a valuable tool for the analysis of the piston ring pack performance. The complex physical phenomena occurring in the cylinder system can be sufficiently described in numerical models and solved in dynamic scenarios to provide useful information concerning the performance and design of the piston ring pack. Such simulations, coupled with modern computational systems and multi-objective optimization techniques are a promising way of understanding and designing such complex systems.

1.2 Piston Ring Pack System Operation Principles

Friction losses , wear patterns, blow-by and oil transportation/scraping in the ring pack are mainly affected by the ring-liner interaction, rings axial and angular motion, ring-groove interaction, gas flow and the piston skirt secondary motion.

1.2.1 Ring Liner Contact

The piston ring pack is usually composed by three rings, namely the compression/top ring, the scraper/second ring and the oil ring. Each ring serve a different function in the ring

pack. The compression ring is designed to handle the high combustion pressure. The oil ring regulates the amount of the lubricating oil flow from the crankcase to the ring liner system. The second ring both regulates the pressure of the combustion chamber and scraps the excessive lubricant oil on the liner.

The ring liner conjunction is a dynamic seal that separates the crankcase from the combustion chamber. In engines with crosshead the ring liner seal is still highly critical to attain high efficiency rates. In order to provide such seal, the rings are pressed outwards by radial forces caused by ring pretension and gas pressure in the region behind the ring. A lubricant oil film between the ring running surface and the cylinder liner provides a wet seal which does not allow gas flow. When the film is disrupted, circumferential flow takes place, increasing the blow-by. Blow-by occurs when undesired combustion gas flows past the ring pack without producing work, diminishing the engine efficiency [11]. In small bore engines blow-by contributes to hydrocarbon and particulate emissions [22].

The lubrication of the ring-liner interface differs with their relative speed. While at midstroke, where the relative speed is high, lubrication is mainly attained by the hydrodynamic wedge effect. As the piston approaches the top dead centre (TDC) and bottom dead centre (BDC) of the engine cycle, its relative speed diminishes and finally comes to a halt. The hydrodynamic wedge effect stops, the film collapses with a transient film-squeeze motion, and mixed or pure boundary lubrication occurs. The asperity contact occurring in TDC and BDC is important for understanding ring and liner wear. Lubricant oil viscosity is an important parameter of the system as high viscosity values result in high friction losses, while low viscosity does not maintain a sufficient hydrodynamic wedge throughout the hydrodynamic lubrication phase.

The ring face profile has a convergent divergent geometry that creates a pressure drop resulting in lubricant film potential rupture due to cavitation [8]. Cavitation is the formation of gas pockets in the fluid when the pressure becomes critically low, either by evaporation of the fluid (vapour cavitation), or by the release of dissolved air in the fluid (gaseous cavitation or aeration) [3]. The air in the lubricant fluid being created by cavitation reduces the effective hydrodynamic wedge.

1.2.2 Motion of the Rings Within the Groove and Gas Flow

Rings are within a circumferential groove on the piston skirt, which has a thin oil film and is designed for allowing gas to flow at the back of the ring to create outwards radial forces. These forces in combination with the ring pretension counteract the forces generated by the hydrodynamical wedge of the lubricant film between the ring running surface and the liner.

The movement of the rings within the groove is being dictated by the complex dynamics mostly created by the gas flow in the ring pack orifices and ring packs, ring-groove asperity/oil contact and inertial forces. Ring twist affect the ring running surface geometry and subsequently the ring-liner interaction, effectively coupling the ring-groove dynamics with the ring-liner lubrication dynamics. Axial motion change the geometry of the ring-groove orifices, affecting the gas flow and the gas pressure generated.

According to Tian [18], ring-groove interaction is critical for understanding oil transport, consumption and degradation, as well as the wear of the ring and the grooves of the ring pack assembly.

1.2.3 Secondary Piston Motion

In an internal combustion engine, the clearance between the piston and the liner allows for tilting and lateral motion. This secondary motion of the piston is caused by the side thrust force exerted through the connecting rod. When the piston collides on the liner, piston slap occurs, a phenomenon that is responsible for most of the noise and vibration in the engine [2]. The tilting motion of the piston weakens the seal of the oil control ring, increasing oil consumption [18].

1.3 Literature Review

Gas flow and ring pack dynamics have extensively been researched by simulation models and experimental studies. Comparison between model predictions and experimental measurements has been conducted in numerous occasions e.g. [12, 18, 20]. Most relevant studies aim to predict blow-by, hydrocarbon emissions, engine efficiency and wear.

The importance of understanding the correlation between design parameters and the ring pack function motivates such research and major advancement has been achieved since the first published work in the mid seventies by Ting and Mayer [21, 20], where an one-dimensional analytical model was developed to calculate bore wear, taking into account gas pressure variations in the ring pack . This study assumed no tilt movement of the ring in the groove. Dowson and Ruddy [4] later developed simulations that included the ring dynamics effects.

Keribar et al. [9] developed a ring pack model which included both the ring dynamics and the gas dynamics in the ring pack system, and was capable of incorporating ring twist, axial displacement, gas pressure values and gas flows. The asperity contact, oil fim squeezing pressures and the ring-liner hydrodynamic and boundary lubrication phenomena

were incorporated in the model. The goal of the study was to predict blowby, cylinder liner friction and the consumption of oil, using a set of submodules which were interrelated and solved together. Each of these submodules solves an aspect of the system. A diagram of the modules and their relations based on that given in [9] is shown in figure 1.1.

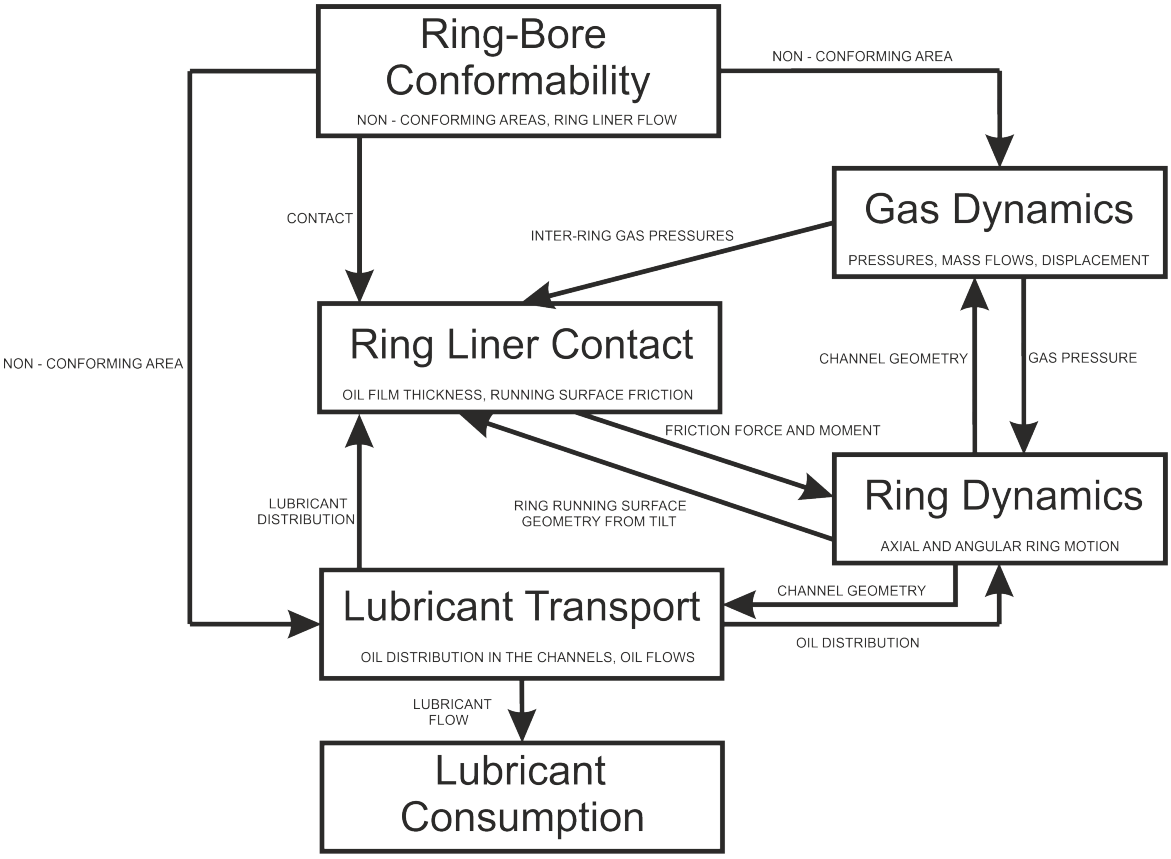

Figure 1.1 Piston Ring Pack Modules of Keribar et al. [9]

However Keribar et al. considered the ring groove channel flows to be orifice flows which is a simplification. Heywood and Namazian [12] developed a ring motion model coupled with a flow model but didn't incorporate the tilting motion of the ring. Tian et al. [19] incorporated ring twisting effects and low Reynolds flows in the ring groove channels.

Non-axissymmetric models such as the one by Liu [11] adress the non-comformability issues and other three dimensional characteristic of the piston ring system.

Chapter 2

Physical Modeling of the Ring Pack System

2.1 Introduction

The second chapter of this thesis concerns the analysis of the physical phenomena taking place in the piston ring pack system model. Additionally, in the current chapter, the formulation of the model is described thoroughly. The model is very much based on the work of Tian [18].

The current model is a two dimensional model of the piston ring pack, which includes the complex interaction of the ring-groove system and the gas flow. The plane of the model is defined by an axis parallel to the piston rod and an axis parallel to the radius of the ring groove. The gas flows through the ring and groove clearances and the pressure of the gas contained in the inter-ring space and in the ring back space are calculated. The circumferential flows and geometry variations are out of the model's limitations and are being neglected. Conformability of the ring on the cylinder liner and variable twist and lift alongside the circumference is also not being taken into account. For these phenomena, a three dimensional model is needed, as the one that has been developed by Liu [11]. However flow through the ring gaps is taken into account in the model.

Namely, the physical phenomena that are being modeled are:

- the gas flow in the orifices and the gas pressure in the chambers of the piston ring pack system
- the gas displacement in the orifices of the piston ring pack system
- interaction of the ring and its groove regarding the oil film contact

- interaction of the ring and its groove regarding the asperity contact
- the inertia forces acting on the system

It is important to emphasize the strong relationship between the ring dynamics and the gas flow calculations, as the movement of the rings in their flanks strongly affect the geometry of the ring-groove channels and subsequently the flow and displacement of the gas.

The input of the model contains variables that depend on phenomena which are not being included in the model. The combustion chamber pressure of the gas at the very top of the ring pack is assumed to be known. The friction force and moment between the rings and the cylinder liner is assumed to be uncoupled with the current model and is also assumed to be known to the system. The temperature of the liner is assumed to be an input as well.

The model provides as an output the tilting and axial displacement (lift) of each ring in its groove at any given crank angle, as well as the pressures and gas flows in every orifice and chamber in the system, including the blow by. The importance of blow by has been extensively discussed in the first chapter. Asperity pressure distribution on the flanks is also an output of the model, providing valuable information regarding the wear of the piston ring.

The design parameters that can be varied include the ring pack's rings and ring groove geometry, ring mass, the ring gap size, the number of the rings, the type of the engine, the viscosity of the oil on the groove and the surface roughness of both the groove and the ring flanks.

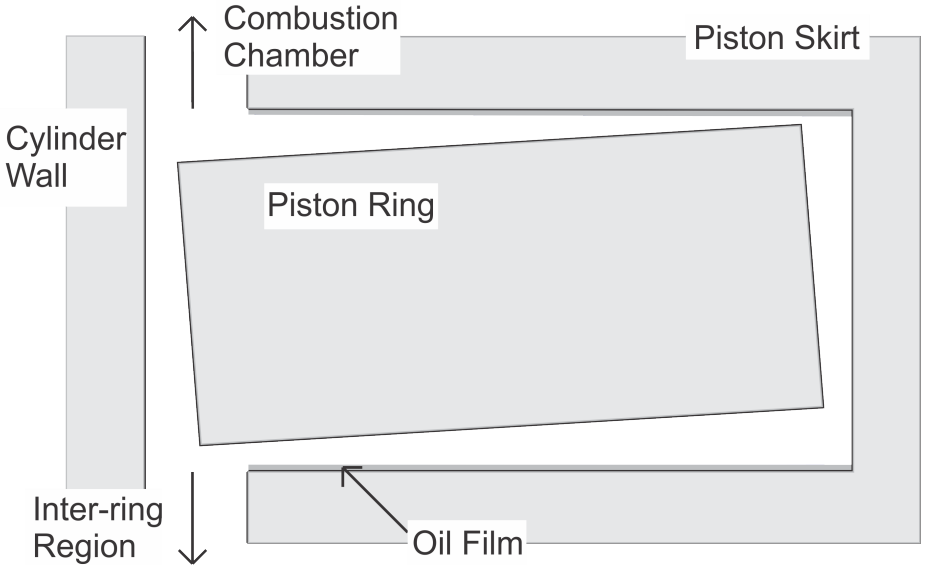

Figure 2.1 Model representation

2.2 Ring-Groove Interaction

2.2.1 Oil Film Calculations

In the piston ring pack system, oil is being accumulated on the flanks of the grooves. For the purpose of this model, an assumption of a oil film on piston grooves is made. The oil film generates pressure when the ring comes in contact with the oil, but only when the ring and groove distance is diminishing.

The distance between the ring and the corresponding groove at the position x and time t when the groove and ring sides are flat with no chamfers and other geometry complexities is:

$$h(x,t) = h_0(t) + a(t)x \tag{2.1}$$

In order to formulate the interaction of the ring with the oil on the groove, the Reynolds equation has been used:

$$\frac{1}{12\mu_{oil}}\frac{\partial}{\partial x}\left(h^3(x,t)\frac{\partial p_{oil}(x,t)}{\partial x}\right) = \frac{\partial h(x,t)}{\partial t} \tag{2.2}$$

Conditions should describe when the oil pressure is being generated. For the distance h(x,t), the conditions for oil pressure generation are:

$$h(x,t) \leq h_{oil} \tag{2.3}$$

$$\frac{\partial h(x,t)}{\partial t} \leq 0 \tag{2.4}$$

At a given time, if the conditions above are met in a region where x is $x_a \leq x \leq x_b$, assuming that the gas pressure before and after the ring-groove channel is p_a and p_b respectively, the boundary conditions of the Reynolds equation are

$$\begin{aligned} p_{oil}(x_a) &= p_a \\ p_{oil}(x_b) &= p_b \end{aligned} \tag{2.5}$$

In order to find the force and moment that is being generated by the oil pressure, the Reynolds equation should be solved for the pressure gradient. Integrating with respect to x, (2.2) yields:

$$\frac{\partial p_{oil}(x,t)}{\partial x} = \frac{12\mu_{oil}}{h^3(x,t)} \int_{x_a}^{x} \frac{\partial h(x,t)}{\partial t} dx + C_0 \tag{2.6}$$

where from (2.1),

$$\frac{\partial h(x,t)}{\partial t} = \frac{dh_0(t)}{dt} + x\frac{da(t)}{dt} \tag{2.7}$$

$$\int_{x_a}^{x} \frac{\partial h(x,t)}{\partial t} dx = \frac{1}{2}(x^2 - x_a^2)\frac{da(t)}{dt} + (x - x_a)\frac{dh_0(t)}{dt} \tag{2.8}$$

In order for the C_0 to be calculated, (2.6) should again be integrated with respect to x:

$$p_{oil}(x,t) = 12\mu_{oil}\left[\frac{1}{2}\frac{da(t)}{dt}\int_{x_a}^{x}\frac{(x^2 - x_a^2)}{h^3(x,t)}dx + \frac{dh_0(t)}{dt}\int_{x_a}^{x}\frac{(x - x_a)}{h^3(x,t)}dx\right] + C_0\int_{x_a}^{x}\frac{1}{h^3(x,t)}dx + C_1 \tag{2.9}$$

and with application of the boundary conditions in (2.5):

$$p_{oil}(x_a) = p_a = C_1 \tag{2.10}$$

$$\begin{aligned} p_{oil}(x_b) = p_b = \\ = 12\mu_{oil}\left[\frac{1}{2}\frac{da(t)}{dt}\int_{x_a}^{x_b}\frac{(x^2 - x_a^2)}{h^3(x,t)}dx + \frac{dh_0(t)}{dt}\int_{x_a}^{x_b}\frac{(x - x_a)}{h^3(x,t)}dx\right] + C_0\int_{x_a}^{x_b}\frac{1}{h^3(x,t)}dx + C_1 \end{aligned} \tag{2.11}$$

the equations above yield:

$$C_0 = \frac{p_b - p_a - 12\mu_{oil}\left[\frac{1}{2}\frac{da(t)}{dt}\int_{x_a}^{x_b}\frac{(x^2 - x_a^2)}{h^3(x,t)}dx + \frac{dh_0(t)}{dt}\int_{x_a}^{x_b}\frac{(x - x_a)}{h^3(x,t)}dx\right]}{\int_{x_a}^{x_b}\frac{1}{h^3(x,t)}dx} \tag{2.12}$$

Now, using (2.6) and (2.12), it is possible to express the force and moment generated by the oil as a function of the ring movement and the gas pressure:

$$\begin{aligned} F_{oil} &= \int_{x_a}^{x_b} p_{oil}(x,t)dx = \int_{x_a}^{x_b}(x - x_a)' p_{oil}(x,t)dx = \Big[(x - x_a)p_{oil}(x,t)\Big]_{x_a}^{x_b} - \int_{x_a}^{x_b}(x - x_a)\frac{\partial p_{oil}}{\partial x}dx \\ &= p_b(x_b - x_a) - \int_{x_a}^{x_b}(x - x_a)\frac{\partial p_{oil}}{\partial x}dx \end{aligned} \tag{2.13}$$

and similarly:

$$M_{oil} = \int_{x_a}^{x_b} x\, p_{oil}(x,t)dx = \frac{1}{2}p_b(x_b^2 - x_a^2) - \frac{1}{2}\int_{x_a}^{x_b}(x^2 - x_a^2)\frac{\partial p_{oil}}{\partial x}dx \tag{2.14}$$

2.2.2 Gas Flow Calculations

In the piston ring pack system, the volume at the back of the ring, and the volume between two consecutive rings, the ring skirt and the cylinder liner, act as chambers. The gas pressure in these chambers generate forces and moments on the rings. These chambers can become connected by three types of channels. The first type of channel is the orifice contained by a ring and its respective groove, which, from this point on, would be referred as a ring groove channel. The second channel type are the ring gaps. The third type has to do with the gas flow through the running surface of the rings on the cylinder liner (circumferential flow). This thesis is concerned only with the first two types of channels. When the channels are open, the pressure difference generates gas flow and in the occasion of the ring groove channel, the gas flow subsequently generates gas pressure on the ring flank.

Flow between a ring and its respective groove flank

In the first section of the chapter, a physical model calculating the oil pressure generation was developed. Oil generates pressure when the ring groove distance is smaller than the film

thickness in a region. In order for the gas to flow in the channel, the distance between the ring and the flank should be greater than the oil film thickness at all positions x. Gas flow and oil pressure contact cannot happen simultaneously.

The gas flow in the ring and groove channel is calculated with the following assumptions (based on [18], [12]):

- The Reynolds number in the channel is low (<2000) and the flow is laminar and fully developed
- The effect created by the ring movement on the gas is not taken into account due to gas' low viscosity
- The gas is incompressible as the gas velocity corresponds to a Mach number value well below 0.3
- Although ring movement exists, its boundary on the flow field is assumed to be constant
- The channel width is much smaller than its length
- The flow is assumed to be parallel although there is an angle between the ring and the groove

These assumptions allow for a Plane Poiseuille Flow implementation in the channel as in [18]:

$$\frac{d^2u(y)}{dy^2} = \frac{1}{\mu_{gas}} \frac{dp_{gas}}{dx} \tag{2.15}$$

Assuming a no slip boundary condition on the ring and groove sides:

$$\begin{aligned} u(0) &= 0 \\ u(h_{gas}(x)) &= 0 \end{aligned} \tag{2.16}$$

Where:

$$h_{gas}(x) = h(x) - h_{oil} \tag{2.17}$$

Integrating 2.15 with respect to y twice:

$$\frac{du(y)}{dy} = \frac{1}{\mu_{gas}} \frac{dp_{gas}}{dx} y + C_0$$
$$u(y) = \frac{1}{2\mu_{gas}} \frac{dp_{gas}}{dx} y^2 + C_0 y + C_1$$

And then applying the boundary condition 2.16:

$$C_0 = 0$$
$$C_1 = \frac{1}{2\mu_{gas}} \frac{dp_{gas}}{dx} h_{gas}$$

Yields the velocity distribution in the channel:

$$u(y) = \frac{1}{2\mu_{gas}} \frac{dp_{gas}}{dx} y(y - h_{gas}) \tag{2.18}$$

For the pressure gradient in the direction parallel to the groove flank the following condition is imposed:

$$\frac{d}{dx}\left(h_{gas}^3(x) \frac{dp_{gas}}{dx} \right) = 0 \tag{2.19}$$

Intergrating with respect to x yields:

$$h_{gas}^3(x) \frac{dp_{gas}}{dx} = C$$

or

$$\frac{dp_{gas}}{dx} = \frac{C}{h_{gas}^3(x)}$$

Integrating again gives the pressure:

$$p_{gas}(x) = C \int_{x_a}^{x} \frac{1}{h_{gas}^3(x)} dx + C_a$$

and using boundary conditions $p_{gas}(x_a) = p_a$ and $p_{gas}(x_b) = p_b$ yields the following:

$$\begin{aligned} C_a &= p_a \\ C &= \frac{p_b - p_a}{\int_{x_a}^{x_b} \frac{1}{h_{gas}^3(x)} dx} \end{aligned}$$

Combining the above, finally, gives the expression for the spacial derivative for the pressure:

$$\frac{dp_{gas}}{dx} = \frac{p_b - p_a}{h_{gas}^3(x) \int_{x_a}^{x_b} \frac{dx}{h_{gas}^3(x)}} \tag{2.20}$$

The volume flow rate is calculated:

$$\begin{aligned} Q &= -\frac{dp_{gas}}{dx} \frac{h_{gas}^3(x)}{12\mu_{gas}} \\ &= -\frac{p_b - p_a}{12\mu_{gas} \int_{x_a}^{x_b} \frac{dx}{h_{gas}^3(x)}} \end{aligned} \tag{2.21}$$

The gas density is approximated as in [18]:

$$\rho_{gas} = \frac{p_a + p_b}{2RT} \tag{2.22}$$

Now using the 2.21 the following expression can be obtained for the mass flow:

$$\dot{m}_{gas} = \frac{p_a^2 - p_b^2}{24\mu_{gas} RT \int_{x_a}^{x_b} \frac{dx}{h_{gas}^3(x)}} \tag{2.23}$$

According to [12], the gas viscosity can be calculated as follows (temperature in K, viscosity in Pa s):

$$\mu_{gas} = 3.3 \times 10^{-7} \times T^{0.7} \tag{2.24}$$

Using the expression for the spacial derivative of the pressure in eq. 2.20 and the boundary condition $p_{gas}(x_a) = p_a$ and integration by parts yields the expressions for the force and moment generated by the gas:

$$F_{gas} = \int_{x_a}^{x_b} p_{gas} dx = p_b(x_b - x_a) - \int_{x_a}^{x_b} (x - x_a) \frac{dp_{gas}}{dx} dx \tag{2.25}$$

$$M_{gas} = \int_{x_a}^{x_b} x p_{gas} dx = \frac{1}{2} p_b(x_b^2 - x_a^2) - \frac{1}{2} \int_{x_a}^{x_b} (x^2 - x_a^2) \frac{dp_{gas}}{dx} dx \tag{2.26}$$

Flow through a Ring Gap

According to [18], [4] and [9] the gas mass flow through the ring gap can be approximated by an isentropic nozzle flow:

$$\dot{m}_{gap} = \frac{C_D A_{gap} p_U}{\sqrt{R T_U}} f_m \tag{2.27}$$

Where p_U and p_D is the pressure of the gas upstream and downstream respectively, A_{gap} is the gap area, T_U is the temperature of the gas upstream and R is the specific gas constant. C_D is the discharge coefficient, obtained by experimental data in[17]:

$$C_D = 0.85 - 0.25 \left(\frac{p_D}{p_U} \right)^2$$

And f_m [18]:

$$f_m = \begin{cases} \gamma^{\frac{1}{2}} \left(\frac{2}{\gamma+1}\right)^{\frac{\gamma+1}{2(\gamma+1)}} & \frac{p_D}{p_U} \leq \left(\frac{2}{\gamma+1}\right)^{\frac{\gamma}{\gamma-1}} \\ \left(\frac{p_D}{p_U}\right)^{\frac{1}{\gamma}} \left\{ \frac{2}{\gamma-1} \left[1 - \left(\frac{p_D}{p_U}\right)^{\frac{\gamma-1}{\gamma}} \right] \right\}^{\frac{1}{2}} & \frac{p_D}{p_U} \geq \left(\frac{2}{\gamma+1}\right)^{\frac{\gamma}{\gamma-1}} \end{cases}$$

2.2.3 Gas Displacement

In [18] Tian states that the volumes contained in the ring groove channel are relatively large. Thus, they can not be neglected due to the corresponding mass variations' influence on the gas pressure in the chambers of the piston ring pack system.

In the gas displacement model the three different possible configurations regarding the ring position in the groove should be considered. The three configurations are:

- When the outer ring edge comes in contact with the oil film and stops the corresponding gas flow
- When the inner ring edge comes in contact with the oil film
- When no contact occurs on either edges

In figures 2.2-2.4 the configurations above are displayed. The distances between the ring and the oil are h_a and h_b, at positions x_a and x_b respectively, a is the tangent of the ring tilting angle with the positive tilting angle shown in the figure.

In the occasion of edge contact when $a < 0$, from the ideal gas law $pV = mRT$, the volume contained in 2.3 $V = h_a(x_b - x_a)$ and $tan(\theta) = a = h_a/(x_b - x_a)$,the following equation can be generated:

$$m_{gd} = -\frac{p_a h_a^2}{2aRT} \tag{2.28}$$

and with differentiation:

$$\dot{m}_{gd} = -\frac{1}{RT}\left(\frac{h_a^2}{2a}\frac{dp_a}{dt} + \frac{h_a p_a}{a}\frac{dh_a}{dt} - \frac{h_a^2 p_a}{2a^2}\frac{da}{dt}\right) \tag{2.29}$$

and in the occasion of edge contact when $a > 0$ 2.4, the equations are:

$$m_{gd} = \frac{p_b h_b^2}{2aRT} \tag{2.30}$$

and

$$\dot{m}_{gd} = \frac{1}{RT}\left(\frac{h_b^2}{2a}\frac{dp_b}{dt} + \frac{h_b p_b}{a}\frac{dh_b}{dt} - \frac{h_b^2 p_b}{2a^2}\frac{da}{dt}\right) \tag{2.31}$$

The implementation in [18] for the configuration where the ring is not in contact with the groove (fig. 2.2) is:

$$m_{gd} = \frac{(p_a h_a + p_b h_b)(x_b - x_a)}{2RT} \tag{2.32}$$

and:

$$\dot{m}_{gd} = \frac{x_b - x_a}{2RT}\left[\left(h_a\frac{dp_a}{dt} + h_b\frac{dp_b}{dt}\right) + \left(p_a\frac{dh_a}{dt} + p_b\frac{dh_b}{dt}\right)\right] \tag{2.33}$$

Tian states that the use of the equations 2.32, 2.33 is driven by the necessity of preserving continuity between the different ring groove configurations. Then, the gas flow causing in the positions x_a and x_b the mass increase is assumed to be proportional to the distances h_a and h_b:

$$\dot{m}_{gda} = \frac{h_a}{h_a + h_b}\dot{m}_{gd} \tag{2.34}$$

and

$$\dot{m}_{gdb} = \frac{h_b}{h_a + h_b}\dot{m}_{gd} \tag{2.35}$$

2.2.4 Asperity Contact Calculations

When the ring groove distance becomes lower than a critical value in a region, asperity contact occurs.

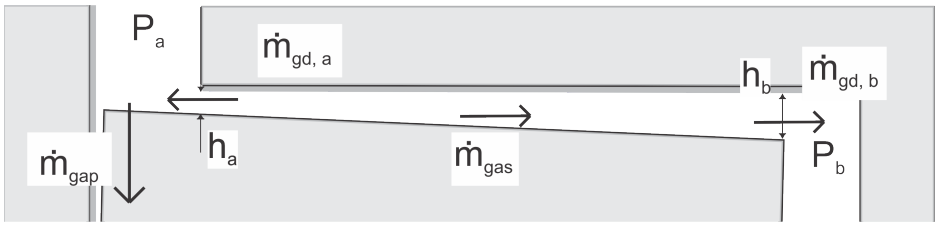

Figure 2.2 Gas displacement with no oil contact

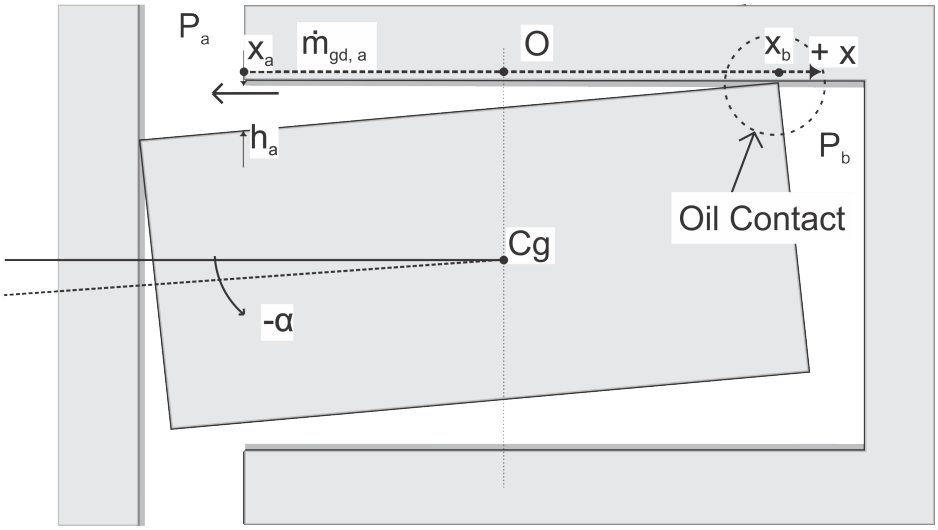

Figure 2.3 Gas displacement with negative twist

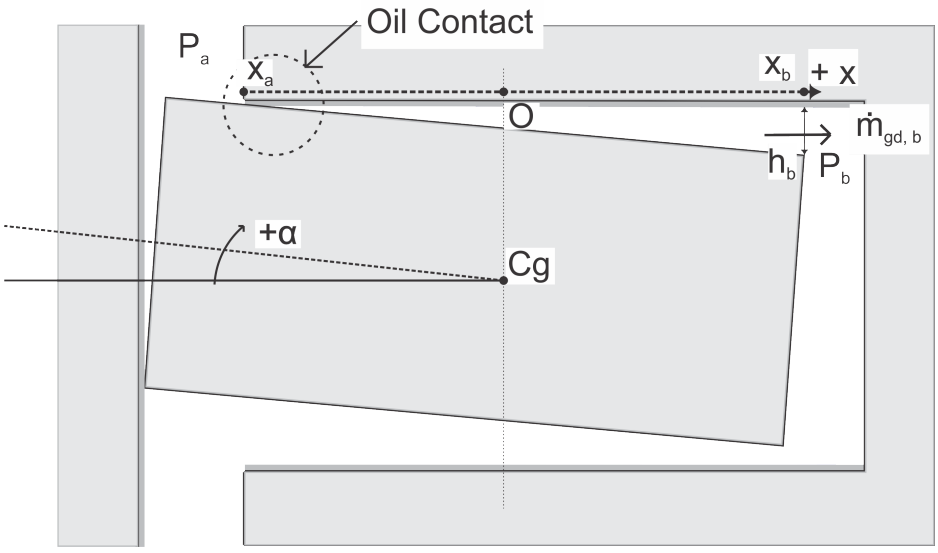

Figure 2.4 Gas displacement with positive twist

The asperity contact model that has been used is the elastic deformation mode of the Greenwood and Tripp [6] model which assumes a Gaussian distribution of the height of the asperities.

The average contact pressure distribution when both surfaces are rough in [6] is given by:

$$p_c = \frac{8\pi}{5}(\eta\beta\sigma)KE'F_{5/2}(\frac{h}{\sigma}) \tag{2.36}$$

where

$$K = \frac{2\sqrt{2}}{3}\pi(\eta\beta\sigma)\sqrt{\frac{\sigma}{\beta}} \tag{2.37}$$

with η being the surface density of asperity peaks, β being the radius of the curvature of the paraboloidal asperities (the shape of the asperity is described as $f(x) = x/b^2$) and σ the variance of the composite surface roughness.

E' is the composite elastic modulus of the two surfaces, which, in this particular occasion, are the ring (E_r,v_r)and the groove (E_f,v_f) flank surfaces:

$$\frac{1}{E'} = \frac{1-v_r^2}{E_r} + \frac{1-v_f^2}{E_f} \tag{2.38}$$

The implementation in [7] is being used in this model:

$$p_c = K'E'F_{5/2}(\frac{h}{\sigma}) \tag{2.39}$$

where:

$$K' = \frac{16\pi}{15}(\eta\beta\sigma)\sqrt{\frac{\sigma}{\beta}} = 2.396 \times 10^{-4} \tag{2.40}$$

and:

$$F_{5/2} = \begin{cases} A(\Omega - \frac{h}{\sigma})^Z & \frac{h}{\sigma} \leq \Omega \\ 0 & \frac{h}{\sigma} > \Omega \end{cases} \tag{2.41}$$

where $\Omega = 4$, $A = 4.4069 \times 10^{-5}$ and $Z = 6.804$.

2.3 Inertia Force

The inertia force acting on each ring in the system can be calculated by the piston acceleration and the ring masses.

For the piston position the equation in [23] is used:

$$x = ((l + r)^2 - o)^{1/2} - (l^2 + (o + rsin\phi)^2)^{1/2} - rcos\phi \tag{2.42}$$

where l is the rod length, r is the crank radius, o is the offset of the pin and ϕ is the crank angle.

The velocity function can then be derived:

$$\dot{x} = r\omega sin\phi + r\omega(o + rsin\phi)cos\phi(l^2 - (o + rsin\phi)^2)^{-1/2}$$

where ω is the rotational speed of the crankshaft.

The acceleration function is:

$$\begin{aligned} \ddot{x} = {} & r\omega^2 cos\phi + (r\omega(o + rsin\phi)cos\phi)^2(l^2 - (o + rsin\phi)^2)^{-3/2} \\ & + ((r\omega cos\phi)^2 - r\omega^2(o + rsin\phi)sin\phi)(l^2 - (o + rsin\phi)^2)^{-1/2} \end{aligned} \tag{2.43}$$

2.4 Other Forces and Moments Acting on the Ring

The pressure calculations in the ring groove channel and the forces and moments that they generate on the ring have been already been presented previously.

The gas pressure acting on the ring back, the pressure on the ring running surface and the gas pressure acting on the part of the ring between the piston skirt and the cylinder liner, generate moments and forces as well.

2.4.1 Moment generated by Radial Pressures Acting on the Ring Back and the Ring Running Surface

In this model, the radial position of each ring is assumed to be constant. This assumption is based on the different order of magnitude between the radial displacement of the ring (in the order of $1\mu m$ [10]) and the axial displacement (in the order of 100 μm [18]).

The radial pressures acting on the ring, however, produce moment that must be considered in the model formulation. The simple ring liner interaction model in [18], couples the ring twist and the corresponding change of the running surface profile of the ring with the moment that the radial pressures generate.

In the Tian model, a variable minimum point of the ring running surface is assumed. This is the point where the ring liner distance is minimum and it varies with the ring twist. Above and below this point, the gas pressure is assumed to be equal to the upper and lower gas pressures respectively. On the back of the ring, the gas pressure generates a force that, considering the constant axial position of the ring, must be counteracted by the upper and lower gas pressures on the ring running surface profile and the pressure at the minimum point. Thus, on this minimum point, it is assumed that any excess of force is concentrated, in order to maintain the equilibrium of forces in the axial direction. This concentrated force F_{radial} on the minimum point x_0 is:

$$F_{radial} = (l_1 + l_2)p_{back} - (l_2 - x_0)p_{upper} - (l_1 + x_0)p_{lower} \tag{2.44}$$

where, as shown in figure 2.5, l_1 and l_2 are the parts of the ring running surface that are above and below the center of gravity of the ring, respectively, p_{back} is the gas pressure acting on the back of the ring, and p_{lower}, p_{upper} are the gas pressures above and below the minimum point x_0, respectively.

Now, for the moment generated on the ring running surface:

$$M_{rs} = \frac{p_{upper}(l_2^2 - x_0^2)}{2} + \frac{p_{lower}(x_0^2 - l_1^2)}{2} + F_{radial}x_0 \tag{2.45}$$

According to Tian, the model is accurate due to the fact that the moment on the ring running surface is important only around the top dead centre of the piston cycle where the gas pressures are high and the oil supply is limited because the oil control ring does not reach the top dead centre positions of the upper rings. In this region, the load of the large gas

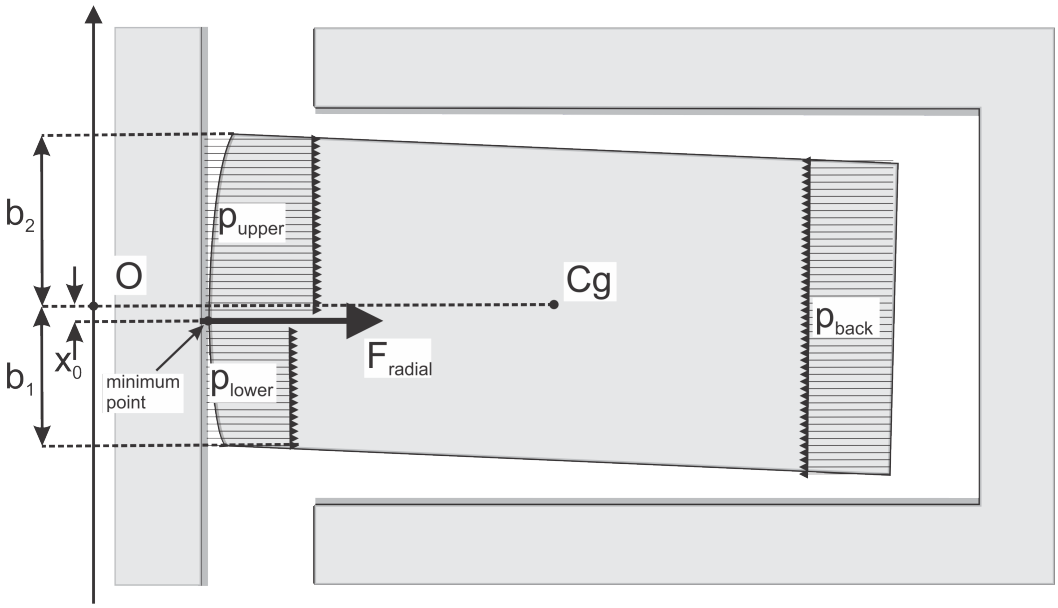

Figure 2.5 Depiction of the radial pressures generating the moment

pressure is being balanced by the hydrodynamic and asperity contact pressure concentrated in the vicinity of the minimum point of the ring running surface.

2.4.2 Moments and Forces Generated by Gas Pressure Between the Piston Skirt and Liner

Gas generates pressure on the part of the ring that protrudes from the groove. The pressure is equal to the pressure of the inter-ring territory or the pressure in the top and bottom piston orifice. The piston skirt and liner distance is this thesis is assumed to be constant and piston secondary motion is not taken into account.

The moments and forces acting on the protruding part of the ring can be simply calculated:

$$F_{sl,u/l} = h_{sl} p_{u/l} \tag{2.46}$$

and

$$M_{sl,u/l} = h_{sl} p_{u/l} (d_{CG} - \frac{h_{sl}}{2}) \tag{2.47}$$

where $p_{u/l}$ is the pressure in the upper and lower territory, respectively,

h_{sl} is the piston skirt and liner distance
d_{CG} is the distance of the ring running surface from the centre of gravity of the ring

2.5 System equations

At each time step a system of equations and unknowns should be fulfilled. These equations are derived from the gas mass conservation in the system and the forces and moments equations. The mass conservation and the equilibrium equations are coupled and are part of the same system. Depending on the number of the rings, the size of the system may vary.

2.5.1 Mass Conservation Equations

As it has been described before in 2.2.2, the inter-ring volumes and the volumes at the ring backs are modeled as gas chambers and the gas pressure in them is assumed to be the same in all of their volume. The volumes are assumed to be constant as the secondary piston motion is not being modeled and the radial ring position is assumed to be constant. Due to the two dimensional nature of the model, the quantities (pressures, masses, etc.) are calculated for a cross-section on the radial-axial plane per unit of circumferential length. Implementing the ideal gas law in such a volume yields:

$$p_i(t)\frac{V_i}{\pi B} = m_i(t)RT_i \tag{2.48}$$

where p_i is the pressure in the volume i, m_i is the mass in the volume, V_i total volume along the circumference, B is the bore diameter, R is the specific gas constant.

With time derivation the following equation is obtained as in [18]:

$$\frac{dp_i}{dt}\frac{V_i}{\pi BRT_i} = \sum \dot{m}_i \tag{2.49}$$

Where for ring back volumes of ring r:

$$\begin{aligned}\sum \dot{m}_i &= \dot{m}_{i,in} - \dot{m}_{i,out} \\ &= \dot{m}_{gas,(i-1,i)} + \dot{m}_{gdb,r,upper} - \dot{m}_{gas,(i,i+1)} - \dot{m}_{gda,r,lower}\end{aligned} \tag{2.50}$$

and for inter-ring volumes between rings r, r+1:

$$\begin{aligned}\sum \dot{m}_i &= \dot{m}_{i,in} - \dot{m}_{i,out} \\ &= \dot{m}_{gas,(i-1,i)} + \dot{m}_{gdb,r,lower} + \dot{m}_{gap,(i-2,i)} - \dot{m}_{gas,(i,i+1)} - \dot{m}_{gdb,r+1,upper} - \dot{m}_{gap,(i,i+2)}\end{aligned} \tag{2.51}$$

where $\dot{m}_{gas,(i,j)}$ is the channel gas flow between volumes i and j,

$\dot{m}_{gd}$ is the gas displacement of upper/lower flank of ring r at the start or the end of the channel (indicated with a and b, respectively) and

$\dot{m}_{gap,(i,j)}$ is the ring gap gas flow between i and j.

All the gas flows are signed.

2.5.2 Forces and Moments Equations

On each ring r from the second Newton's law in the axial direction:

$$\sum F_{axial,r} = \frac{m_r}{\pi B}\frac{d^2h(t)_r}{dt^2} \tag{2.52}$$

or

$$\begin{aligned}\frac{m_r}{\pi B}\frac{d^2h(t)_r}{dt^2} = F_{gas,u} - F_{gas,l} + F_{oil,u} - F_{oil,l} + F_{asp,u} - F_{asp,l} \\ +F_{sl,u} - F_{sl,l} + F_{rl,r} + F_{inertia,r} + W_r\end{aligned} \tag{2.53}$$

where u and l indicate the upper and lower flank, respectively,

m_r is the total mass of the ring r,

$h(t)_r$ is the axial position of the ring r,

B is the cylinder bore diameter,

F_{gas} is the force generated by the gas,

F_{oil} is the force generated by the oil on the groove flank,

F_{asp} is the force generated by the asperity contact between the ring and the groove,

F_{sl} the force acting on the protruding part of the ring between the piston skirt and the cylinder liner

F_{rl} is the friction force generated between the ring running surface and the cylinder liner,

$F_{inertia}$ is the inertia force due to the piston acceleration,

W is the weight force, $W = \frac{m_r}{\pi B}g$ if the piston is at a transverse position.

And for the moments:

$$\sum M_r = \frac{I_r}{\pi B}\frac{d^2 a(t)_r}{dt^2} \tag{2.54}$$

or

$$\frac{I_r}{\pi B}\frac{d^2 a(t)_r}{dt^2} = M_{gas,u} + M_{gas,l} + M_{oil,u} + M_{oil,l} + M_{asp,u} + M_{asp,l} + F_{rl,r} d_{CG,r} + M_{rs,r} + M_{tors} \tag{2.55}$$

where M_{gas}, M_{oil}, M_{asp} are moments created between the ring and the groove from gas pressure, oil pressure and asperity pressure, respectively,

M_{sl} the moment acting on the protruding part of the ring between the piston skirt and the cylinder liner

I_r is the moment of inertia of the ring r,

$a(t)_r$ is the twist angle of the ring r

$d_{CG,r}$ is the distance of the minimum point of the ring running surface from the center of gravity of the ring r,

$M_{rs,r}$ is the moment generated by pressure acting on the ring back and the ring running surface,

M_{tors} is the moment created by the torsional deformation of the ring, which is according to [18]

$$M_{tors} = (a(t)_r - a_{r,0})T_r = (a(t)_r - a_{r,0})E_r r_w^3 ln\Big(\frac{D_{r,outer}}{D_{r,inner}}\Big)\frac{1}{3(D_{r,outer} + D_{r,inner})} \tag{2.56}$$

where $a_{r,0}$ is the static twist of the ring r,

T_r is the torsional stiffness of ring r,

E_r is the elastic modulus of ring r,

r_w is the width of the ring r,

$D_{r,outer}$ and $D_{r,inner}$ are the outer and inner diameter of ring r, respectively.

In the figure below (fig. 2.6), the entirety of the forces and moments acting on the ring are being presented.

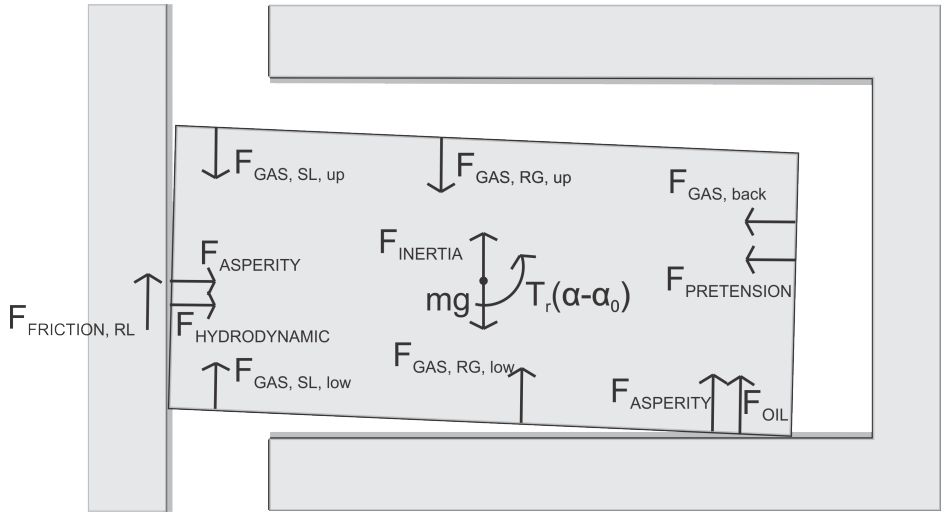

Figure 2.6 Forces acting on the ring

Chapter 3

Computational Model

3.1 Numerical Formulation

In section 2.5, a system of equations physically describing the ring pack model at each time step was presented. This system of equations is effectively coupling the mass conservation equations with the forces and moments equations in the ring pack model. Such a system is strongly non-linear, and an appropriate numerical method should be used to solve it for each time step. In this section the discretised, normalised and non-dimensionalised numerical form of the equations will be presented in detail.

As in [18] the system of equations is formulated in a way so that it is first order in time, in order to achieve numerical stability. For that reason, the axial and angular velocities are considered as system variables, adding two extra variables and equations per ring:

$$\begin{aligned} v(t)_r &= \dot{h}(t)_r = \frac{dh(t)_r}{dt} \\ \omega(t)_r &= \dot{a}(t)_r = \frac{da(t)_r}{dt} \end{aligned} \tag{3.1}$$

The system variables are the axial and angular positions and velocities of the rings, as long as, the pressures in the ring back and the interring volumes.

The axial displacement is the distance between the lower flank of the ring and the groove at the point O identified by the projection of the centre of gravity of the ring on the ring flank (3.1). The ring is not considered to be a rectangular, but it consists of two parallel lines that rotate around the point O. This assumption is reasonable for small angles ϕ where $\sin\phi = \phi$.

Each ring-groove channel has a local coordinate system (3.1) with local variables that can be translated to the system variables. The x axis of the local coordinate system is identified by

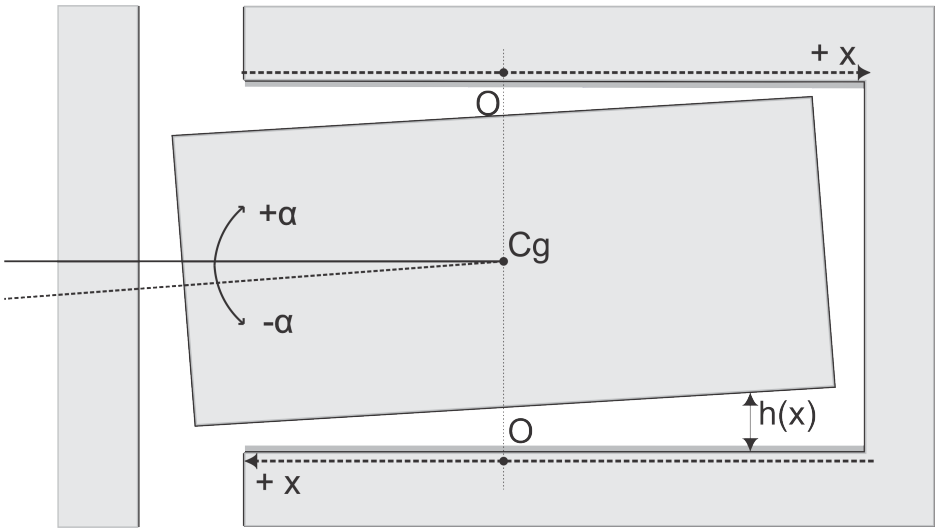

Figure 3.1 Coordinate system of the ring

the groove flank and the origin point is the same as the point O where the axial displacement is measured from. For a lower channel the direction of the axis is from the inner to the outer ring flank edge, as opposed to an upper channel, where the direction of the axis is from the outer ring flank edge to the inner one. The twist angle is positive when the outer edge is higher (closer to the combustion chamber) than the inner edge. The local and global twist angle is the same due to the way the local coordinate systems are established. The same applies to the angular velocity. On the other hand, the local axial distance of the ring from the groove flank at position O is different at the upper and lower flank:

$$h_0(t)_{fl,r} = (w_{g,r} - w_{r,r})(1 - fl) + (-1)^{fl+1} h(t)_r \tag{3.2}$$

and for the axial velocity:

$$v_0(t)_{fl,r} = (-1)^{fl+1} v(t)_r \tag{3.3}$$

where $g_{w,r}$ is the groove width of ring r,

$r_{w,r}$ is the ring width of ring r,

fl is equal to 0 for the upper flank and equal to 1 for the lower flank.

Now, from all the above, the distance between the ring and the groove $h(x,t)_{fl,r}$ can be written as:

$$h(x,t)_{fl,r} = h_0(t)_{fl,r} + a(t)_r x \qquad X_1 \leq x \leq X_2 \tag{3.4}$$

where x is bounded by the ring flank edges, $X_1 = -r_d/2$ and $X_1 = r_d/2$, r_d being the depth of ring r.

The derivative of 3.4 with respect to time yields:

$$\frac{dh(x,t)_{fl,r}}{dt} = (-1)^{fl+1} v(t)_r + \omega(t)_r x \qquad X_1 \leq x \leq X_2 \tag{3.5}$$

Based on [18], h_{ref} and d_{ref} are introduced in order to non-dimensionalise and normalise the radial and axial axes for numerical stability. The same is done for the time with the time step unit δt. By applying these units to 3.4 and 3.5 the following equations are obtained:

$$\begin{aligned} &\frac{h(x,t)_{fl,r}}{h_{ref}} = \frac{h_0(t)_{fl,r}}{h_{ref}} + a(t)_r \frac{1}{(\frac{h_{ref}}{d_{ref}})} \frac{x}{d_{ref}} \Rightarrow \\ &h(x,t)_{n,fl,r} = h_0(t)_{n,fl,r} + a(t)_{n,r} x_n \qquad X_{n,1} \leq x_n \leq X_{n,2} \end{aligned} \tag{3.6}$$

and

$$\begin{aligned} &\frac{dh(x,t)_{fl,r}}{dt} \Big/ \frac{h_{ref}}{\delta t} = (-1)^{fl+1} v(t)_r \Big/ \frac{h_{ref}}{\delta t} + \frac{x}{d_{ref}} \omega(t)_r \Big/ \frac{(\frac{h_{ref}}{d_{ref}})}{\delta t} \Rightarrow \\ &\frac{dh(x,t)_{n,fl,r}}{dt} = (-1)^{fl+1} v(t)_{n,r} + \omega(t)_{n,r} x_n \qquad X_{n,1} \leq x_n \leq X_{n,2} \end{aligned} \tag{3.7}$$

where 3.6 is derived from 3.4 by dividing both members with h_{ref} and 3.7 is derived from 3.5 by dividing both members with $h_{ref}/\delta t$. The subscript n notates that the variable is non-dimensionalised.

When the non-dimensional distance between the ring and the oil film on the groove is needed for gas calculations, for film thickness h_{oil}, the following equation is being used:

$$h_{gas,n} = h_n - h_{n,oil} \tag{3.8}$$

where $h_{n,oil} = h_{oil}/h_{ref}$.

3.2 Mass Conservation Equations in Numerical Form

Writing eqs. 2.50 and 2.51 in non-dimensionalised, normalised and discretised form yields the following equations.

For ring back volumes of ring r where p_1 is the upper pressure of the ring, p_2 is the pressure behind the ring and p_3 is the pressure lower of the ring:

$$\frac{N_{12}\lambda_{u,r,ba}}{M}[p_1(t) - p_1(t-\delta t)] + \left[1 + \left(\frac{N_{12}\lambda_{u,r,bb} + N_{23}\lambda_{l,r,aa}}{M}\right)\right][p_2(t) - p_2(t-\delta t)]$$
$$+\frac{N_{23}\lambda_{l,r,ab}}{M}[p_3(t) - p_3(t-\delta t)] + Q(R_{12}\dot{m}_{u,r,n} - R_{23}\dot{m}_{l,r,n} + N_{12}\kappa_{u,r,b} + N_{23}\kappa_{l,r,a}) = 0 \tag{3.9}$$

For volumes between rings r and $r+1$ where p_1 is the pressure behind ring r, p_2 is the interring pressure and p_3 is the pressure behind ring $r+1$:

$$\frac{N_{12}\lambda_{l,r,ba}}{M}[p_1(t) - p_1(t-\delta t)] + \left[1 + \left(\frac{N_{12}\lambda_{l,r,bb} + N_{23}\lambda_{u,r+1,aa}}{M}\right)\right][p_2(t) - p_2(t-\delta t)]$$
$$+\frac{N_{23}\lambda_{u,r+1,ab}}{M}[p_3(t) - p_3(t-\delta t)] +$$
$$Q(R_{12}\dot{m}_{l,r,n} - R_{23}\dot{m}_{u,r+1,n} + N_{12}\kappa_{l,r,b} + N_{23}\kappa_{u,r+1,a} + \dot{m}_{gap,r} - \dot{m}_{gap,r+1}) = 0 \tag{3.10}$$

where

$$N_{i,j} = \frac{\pi B d_{ref} h_{ref} p_0}{\delta t R \left(\frac{T_i + T_j}{2} \right)}$$

$$M = \frac{V_2 p_0}{\delta t R T_2}$$

$$R_{i,j} = \frac{\pi B h_{ref}^2 p_0^2}{12 d_{ref} R \left(\frac{T_i + T_j}{2} \right) \mu_{gas,i,j}}$$

$$Q = \frac{\delta t}{M}$$

with T_i being the gas temperature of volume i,

V_i being the actual volume of volume i,

B being the bore diameter of the cylinder,

R is the specific gas constant,

$\mu_{gas,i,j}$ being the gas viscosity between volumes i and j, given by eq. 2.24 if $T = (T_i + T_j)/2$,

and $\lambda_{fl,r,ij}$ are the coefficients for the pressure variation terms of the gas displacement equations in flank $fl = u/l$ of ring r, given by eqs. 3.24-3.27,

$\kappa_{fl,r,i}$ are the coefficients for the spacial terms of the gas displacement equations in flank $fl = u/l$ of ring r, given by eqs. 3.24-3.27,

$\dot{m}_{fl,r,n}$ is the non-dimensional mass flow in flank $fl = u/l$ of ring r, given by eq. 3.28,

$\dot{m}_{gap,r}$ is the flow through the gap of ring r given by eq. 2.27

The pressures p_i here are non-dimensionalised, given by the actual pressures being divided by p_0.

3.3 Oil and Gas Forces and Moments in the Ring and Groove Channel

When the ring is not in contact with the oil the force and moment generated $F_{n,og}$ and $M_{n,og}$ is only due to the gas pressure and is obtained by 2.25 and 2.26:

$$F_{n,og} = p_a \frac{\int_{X_{n,1}}^{X_{n,2}} \frac{x_n - X_{n,1}}{h_{gas,n}^3}}{\int_{X_{n,1}}^{X_{n,2}} \frac{1}{h_{gas,n}^3}} + p_b \frac{\int_{X_{n,1}}^{X_{n,2}} \frac{X_{n,2} - x_n}{h_{gas,n}^3}}{\int_{X_{n,1}}^{X_{n,2}} \frac{1}{h_{gas,n}^3}} \tag{3.11}$$

$$M_{n,og} = \frac{p_a}{2} \frac{\int_{X_{n,1}}^{X_{n,2}} \frac{x_n^2 - X_{n,1}^2}{h_{gas,n}^3}}{\int_{X_{n,1}}^{X_{n,2}} \frac{1}{h_{gas,n}^3}} + \frac{p_b}{2} \frac{\int_{X_{n,1}}^{X_{n,2}} \frac{X_{n,2}^2 - x_n^2}{h_{gas,n}^3}}{\int_{X_{n,1}}^{X_{n,2}} \frac{1}{h_{gas,n}^3}} \tag{3.12}$$

the pressures p_a and p_b are non-dimensionalised from here on, using p_0 as the unit of pressure.

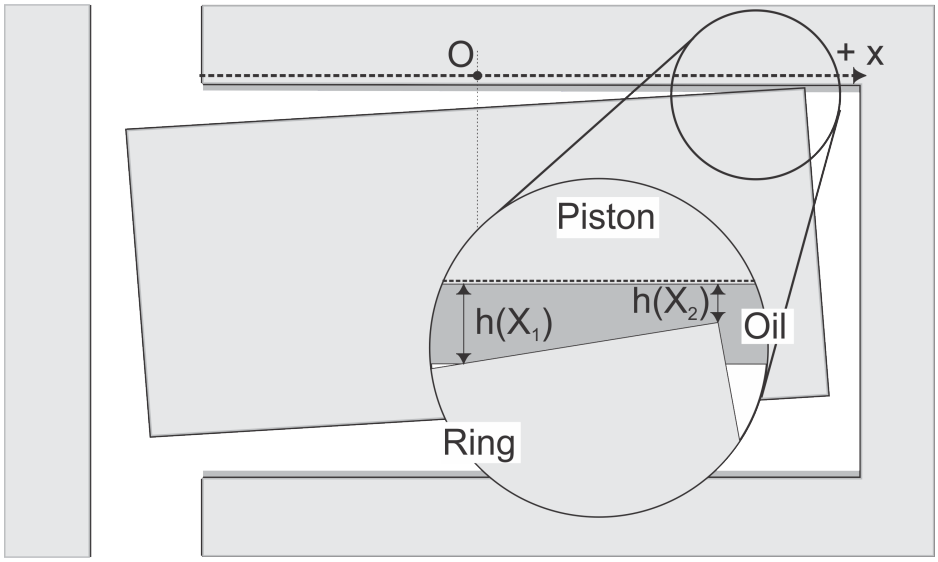

Figure 3.2 Oil contact

When there is ring oil contact in a region between positions $x_{n,oc,1}$ and $x_{n,oc,2}$, which are contained by the ring edges $X_{n,1}$ and $X_{n,2}$ (fig. 3.2), the force and moment on the ring, according to [18], are:

$$F_{n,og} = F_{n,gas} + F_{n,oil} \tag{3.13}$$

$$M_{n,og} = M_{n,gas} + M_{n,oil} \tag{3.14}$$

The gas pressure is generated outside the oil contact region giving:

$$F_{n,gas} = (X_{n,1} - x_{n,oc,1})p_a + (x_{n,oc,2} - X_{n,2})p_b \tag{3.15}$$

and

$$M_{n,gas} = \frac{1}{2}(X_{n,1}^2 - x_{n,oc,1}^2)p_a + \frac{1}{2}(x_{n,oc,2}^2 - X_{n,2}^2)p_b \tag{3.16}$$

The $x_{n,oc,1}$ and $x_{n,oc,2}$ are defined by the movement of the ring and the film thickness. If there are $x^*_{n,oc,1}$ and $x^*_{n,oc,2}$ for which:

$$\begin{cases} x^*_{n,oc,1} = X_{n,1} \\ x^*_{n,oc,2} = min\left(\dfrac{h_{n,oil} - h_{n,0}}{a_n}, X_{n,2}\right) \end{cases} \qquad if \quad a_n > 0 \tag{3.17a}$$

$$\begin{cases} x^*_{n,oc,1} = min\left(\dfrac{h_{n,oil} - h_{n,0}}{a_n}, X_{n,1}\right) \\ x^*_{n,oc,2} = X_{n,2} \end{cases} \qquad if \quad a_n < 0 \tag{3.17b}$$

The $x_{n,oc,1}$ and $x_{n,oc,2}$ can now be defined by the direction in which the ring moves:

$$if \begin{cases} v_{n,0} + x^*_{n,oc,1}\omega_n < 0 \\ v_{n,0} + x^*_{n,oc,2}\omega_n < 0 \end{cases} \quad then \quad \begin{cases} x_{n,oc,1} = x^*_{n,oc,1} \\ x_{n,oc,2} = x^*_{n,oc,2} \end{cases} \tag{3.18a}$$

$$if \begin{cases} v_{n,0} + x^*_{n,oc,1}\omega_n > 0 \\ v_{n,0} + x^*_{n,oc,2}\omega_n < 0 \end{cases} \quad then \quad \begin{cases} x_{n,oc,1} = -v_n/\omega_n \\ x_{n,oc,2} = x^*_{n,oc,2} \end{cases} \tag{3.18b}$$

$$if \begin{cases} v_{n,0} + x^*_{n,oc,1}\omega_n < 0 \\ v_{n,0} + x^*_{n,oc,2}\omega_n > 0 \end{cases} \quad then \quad \begin{cases} x_{n,oc,1} = x^*_{n,oc,1} \\ x_{n,oc,2} = -v_n/\omega_n \end{cases} \tag{3.18c}$$

$$if \begin{cases} v_{n,0} + x^*_{n,oc,1}\omega_n > 0 \\ v_{n,0} + x^*_{n,oc,2}\omega_n > 0 \end{cases} \quad then \quad \begin{cases} x_{n,oc,1} = x_{n,oc,2} = X_{n,1} \quad if \omega_n < 0 \\ x_{n,oc,1} = x_{n,oc,2} = X_{n,2} \quad if \omega_n > 0 \end{cases} \tag{3.18d}$$

In the event of 3.18d the oil generates no pressure because the ring is moving away from the oil at all positions. The effect of suction has not been taken into account in this model.

The oil pressure force and moment equations are given by 2.13 and 2.14:

$$F_{n,oil} = p_b(x_{n,oc,2} - x_{n,oc,1}) - 12\mu_{n,oil}\left(v_0(t)_n I_0 + \frac{1}{2}\omega(t)_n I_1\right) - C_0 I_2 \tag{3.19}$$

and

$$M_{n,oil} = \frac{1}{2}p_b(x^2_{n,oc,2} - x^2_{n,oc,1}) - \frac{1}{2}12\mu_{n,oil}\left(v_0(t)_n I_1 + \frac{1}{2}\omega(t)_n I_3\right) - \frac{1}{2}C_0 I_4 \tag{3.20}$$

where

$$C_0 = \frac{p_b - p_a - 12\mu_{n,oil}\left(v_0(t)_n I_2 + \frac{1}{2}\omega(t)_n I_4\right)}{I_5}$$

$$I_0 = \int_{x_{n,oc,1}}^{x_{n,oc,2}} \frac{(x - x_{n,oc,1})^2}{h(x,t)_n} dx$$

$$I_1 = \int_{x_{n,oc,1}}^{x_{n,oc,2}} \frac{(x^2 - x_{n,oc,1}^2)(x - x_{n,oc,1})}{h(x,t)_n} dx$$

$$I_2 = \int_{x_{n,oc,1}}^{x_{n,oc,2}} \frac{(x - x_{n,oc,1})}{h(x,t)_n} dx$$

$$I_3 = \int_{x_{n,oc,1}}^{x_{n,oc,2}} \frac{(x^2 - x_{n,oc,1}^2)^2}{h(x,t)_n} dx$$

$$I_5 = \int_{x_{n,oc,1}}^{x_{n,oc,2}} \frac{1}{h(x,t)_n} dx$$

$$\mu_{n,oil} = \mu_{oil} \frac{d_{ref}^2}{p_0 h_{ref}^2 \delta t}$$

3.4 Asperity Contact Forces and Moments between the Ring and the Groove

In the asperity contact model that has been presented in section 2.2.4, asperity contact occurs where the distance between the ring and the groove is smaller than 4σ in a region (see eq. 2.41), where σ is the variance of the composite surface roughness. The region in which asperity contact occurs is assumed to be bound by positions $x_{n,ac,1}$ and $x_{n,ac,2}$, that are defined as:

$$\begin{cases} x_{n,ac,1} = X_{n,1} \\ x_{n,ac,2} = min\left(\frac{4\sigma - h_0}{a}, X_{n,2}\right) \end{cases} \qquad if \quad a_n > 0 \tag{3.21a}$$

$$\begin{cases} x_{n,ac,1} = min\left(\frac{4\sigma - h_0}{a}, X_{n,1}\right) \\ x_{n,ac,2} = X_{n,2} \end{cases} \qquad if \quad a_n < 0 \tag{3.21b}$$

Now, with the use of 2.39 the forces and moments due to asperity contact are:

$$F_{asp} = \int_{x_{n,ac,1}}^{x_{n,ac,2}} p_c dx = K' E' A \int_{x_{n,ac,1}}^{x_{n,ac,2}} \left(4 - \frac{h_0 + ax}{\sigma}\right)^z dx \tag{3.22}$$

and

$$M_{asp} = \int_{x_{n,ac,1}}^{x_{n,ac,2}} x p_c dx = K' E' A \int_{x_{n,ac,1}}^{x_{n,ac,2}} x \left(4 - \frac{h_0 + ax}{\sigma}\right)^Z dx \tag{3.23}$$

where, as described in 2.2.4, $K' = 1.198 \times 10^{-4}$, $A = 4.4069 \times 10^{-5}$, $Z = 6.804$ and E' is the combined elastic modulus of the two surfaces (eq. 2.38).

3.5 Mass Flow due to Gas Displacement

The equations 2.28-2.35 in 2.2.3 can be written in the following form in order to uncouple terms containing time derivatives of the pressure variation and terms containing spacial derivatives. According to [18]:

$$\dot{m}_{gda} = \lambda_{aa} \frac{dp_a}{dt} + \lambda_{ab} \frac{dp_b}{dt} + \kappa_a \tag{3.24a}$$

$$\dot{m}_{gdb} = \lambda_{ba} \frac{dp_a}{dt} + \lambda_{bb} \frac{dp_b}{dt} + \kappa_b \tag{3.24b}$$

where λ and κ are defined according to the three different possible ring configurations described in 2.2.3.

If the edge of the ring x_a (inner edge for lower flank or outer edge for upper flank) is in contact with the oil on the groove:

$$\lambda_{aa} = -\frac{h_a^2}{a} \qquad \lambda_{ab} = \lambda_{ba} = \lambda_{bb} = 0 \tag{3.25a}$$

$$\kappa_a = -\frac{h_a p_a}{a}\frac{dh_a}{dt} + \frac{h_a^2 p_a}{2a^2}\frac{da}{dt} \qquad \kappa_b = 0 \tag{3.25b}$$

If the edge of the ring x_b (inner edge for upper flank or outer edge for lower flank) is in contact with the oil on the groove:

$$\lambda_{bb} = \frac{h_b^2}{a} \qquad \lambda_{ab} = \lambda_{ba} = \lambda_{aa} = 0 \tag{3.26a}$$

$$\kappa_a = 0 \qquad \kappa_b = \frac{h_b p_b}{a}\frac{dh_b}{dt} - \frac{h_b^2 p_b}{2a^2}\frac{da}{dt} \tag{3.26b}$$

If neither of the edges of the ring is in contact with the oil on the groove:

$$\lambda_{aa} = \frac{(x_b - x_a)h_a^2}{2(h_a + h_b)} \tag{3.27a}$$

$$\lambda_{ab} = \lambda_{ba} = \frac{(x_b - x_a)h_a h_b}{2(h_a + h_b)} \tag{3.27b}$$

$$\lambda_{bb} = \frac{(x_b - x_a)h_b^2}{2(h_a + h_b)} \tag{3.27c}$$

$$\kappa_a = \frac{h_a(x_b - x_a)}{2(h_a + h_b)}\left(p_a\frac{dh_a}{dt} + p_b\frac{dh_b}{dt}\right) \tag{3.27d}$$

$$\kappa_b = \frac{h_b(x_b - x_a)}{2(h_a + h_b)}\left(p_a\frac{dh_a}{dt} + p_b\frac{dh_b}{dt}\right) \tag{3.27e}$$

where $h_a = h_{n,gas}(x_a)$ and $h_b = h_{n,gas}(x_b)$. x_a can either be $X_{n,1}^{lower}$ or $X_{n,2}^{upper}$ and x_b can either be $X_{n,2}^{lower}$ or $X_{n,1}^{upper}$.

3.6 Mass Flow Through the Ring Groove Channel

By writing the eq. 2.23 in non-dimensional form, the following equation is obtained for the mass flow through the ring groove channel:

$$\dot{m}_n = \frac{p_b^2 - p_a^2}{2 \int_{X_{n,1}}^{X_{n,1}} h(x,t)_{n,fl,r} dx} \tag{3.28}$$

Chapter 4

Model Application

4.1 Case Study

A simplified version of the algorithm developed and described in Chapter 3 has been implemented in a test case, in order to assess the model's capability of predicting the forces and moments acting on the ring, as well as gas flows in the various segments of the piston ring assembly. The simplification is significant but necessary in order for the model to be validated modularly.

In detail, the simplified model receives the piston ring motion and region pressures as an input and yields the gas, asperity and oil forces, pressure distributions and moments, as well as mass flow rates at the ring gap and the ring-groove channels. The mass flow rate due to gas displacement at the ring-groove channels was not calculated due to the lack of validation data.

The data for the validation study have been obtained from the works of Tian [18] and Noordzij [13], regarding a 2 liter, 4-stroke gasoline engine under wide open throttle condition (full load) at $2000 RPM$. This particular test case has been chosen for a number of reasons:

- In the present thesis, the model that has been developed is effectively an implementation of the model described by Tian in [18].
- The results and calculations of Tian's model have been experimentally validated by Noordzij's in [13].
- The necessary information regarding this specific test case for the gasoline engine is given or can be deduced with sufficient accuracy.
- The wide open throttle condition is chosen over the closed throttle condition due to the significantly less transient phenomena that take place in the former. Furthermore,

Table 4.1 Case study parameters

Model parameter	Value
Ring Width r_w [mm]	2.7
Ring Depth r_d [mm]	3.21
Ring Gap Area A_{gap} [mm]	0.35
Ring and Groove Young's Modulus E_r, E_g [GPa]	210
Ring and Groove Poisson's Ratio v_r, v_g	0.3
Groove Width g_w [mm]	2.8
Oil film thickness on the groove h_{oil} [μm]	2
Variance of the combined composite surface roughness σ [μm]	0.5
Specific Ideal gas law constant R' [$m^3\ PaK^{-1}kg^{-1}$]	284.53
Cylinder Bore Diameter B [mm]	82.7
Temperature of gas and oil T [K]	443
Adiabatic index γ	1.4
Rounds per minute RPM	2000
Oil dynamic viscosity $\mu_{oil}[Pa\ s]$	0.0001

the wide open throttle condition is considered more general, and the pressure and flow rate magnitudes are substantial and eligible for comparison.

In this section, any referenced graph or information is obtained by the above mentioned studies.

4.1.1 Data

The necessary model parameters regarding the case study are listed in table 4.1.

The various graphs and information in the work of T.Tian and L.B.Noordzij do not provide directly the entirety of the necessary data required for the validation study. Therefore, certain methodologies have been adopted to extract the data that are given indirectly or cannot be easily acquired with sufficient accuracy. The various quantities and the respective methodology used are presented in the following sections.

Cylinder Pressure

In Tian's wotk [18], the experimentally measured cylinder pressure is presented, along with the calculated pressures in the inter-ring regions. However, the cylinder's gas chamber pressure values are not shown between crank angles $326deg$ and $440deg$ for the wide open throttle condition. In the graph, effectively, the values of the cylinder pressure that exceed $10bar$, are not shown, in order for the cylinder pressure and the rest of the pressures in the inter-

ring volumes to be presented in the same plot and with the same order of magnitude. For a quantitative comparison, in [13], chapter 6, Noordzij presents that, while the cylinder pressure reaches values of $42 - 45bar$, the region between the first and the second ring does not develop pressures that exceed $3bar$.

In order to obtain the cylinder pressure, the graph for the mass flow in chapter 3 in [18] and the aforementioned graph presenting the gas pressure in the region under the top ring are utilized. Now, using eq. 2.27 which expresses the mass flow rate of the gas through the ring gap as a function of the upper(cylinder) and lower(under the top ring) pressure, the cylinder pressure can be approximated with an iterative procedure.

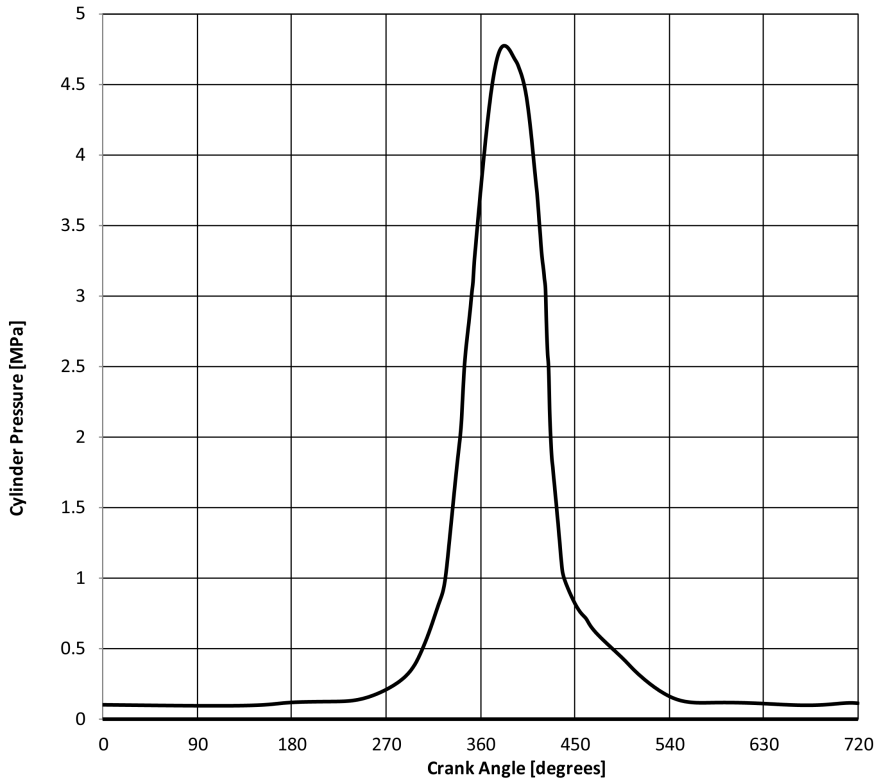

Figure 4.1 Cylinder Pressure

The iterative procedure starts with an initial estimation of the cylinder pressure, utilizing the parts of the graph that are shown (outside crank angles $326deg$ and $440deg$). With an algorithm that solves for each crank angle, using eq. 2.27, the gap flow is calculated and then plotted alongside the gap flow provided by Tian. Then, the cylinder pressure is multiplied by a factor proportional to the deviation between the two flows. The new values of the cylinder pressures are then given to the algorithm as input and the procedure is iterated until a sufficient approximation of the ring gap flow is reached (fig. 4.1).

Ring Motion

Ring motion is described by the distance between the centre of its lower flank and the ring groove (axial displacement or lift), and by its twist (angular displacement). These variables are acquired by a number of graphs in [18]. The axial displacement of the centre of the ring flank is provided in graphical form. However, the accuracy of the graph is not sufficient to describe ring motion in the oil and asperity contact regions. For this purpose, the graphs that present the position of the edges of the ring both at a scale in the order of magnitude of the maximum relative displacement and at a scale in the order of magnitude of the oil film thickness are utilized. From snapshots of the ring edge profile, and by taken into consideration that the ring depth r_d, given in [13], is $r_d = 0.00321m$, an accurate value for the angular displacement can be obtained. These data are then combined to produce a final accurate set of data for the ring motion over a full engine cycle (fig. 4.2 and fig. 4.3).

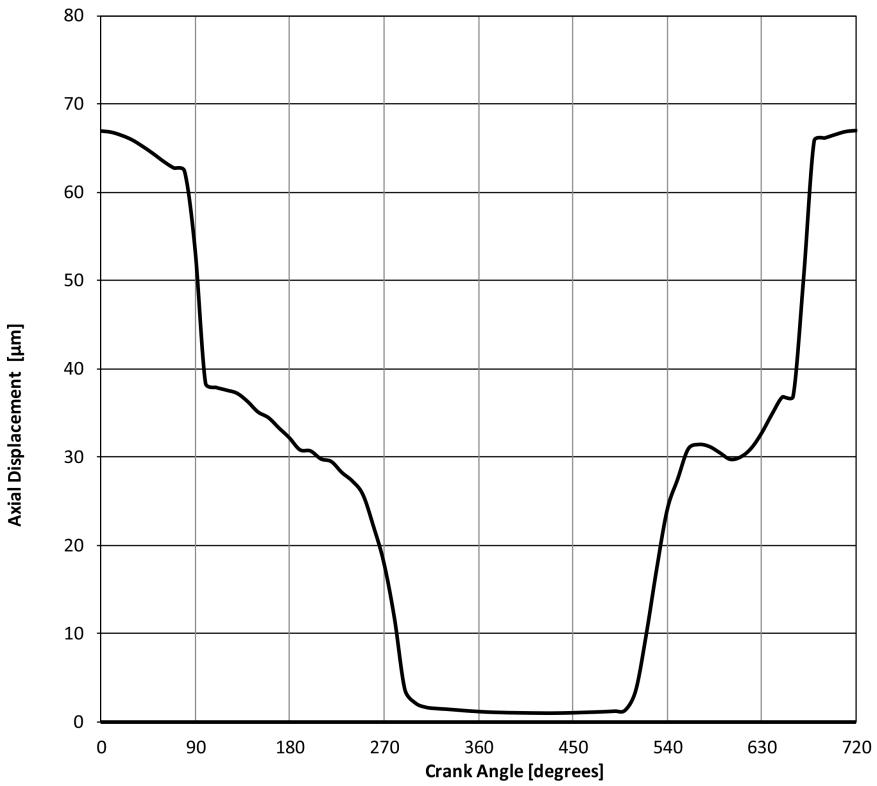

Figure 4.2 Axial Displacement

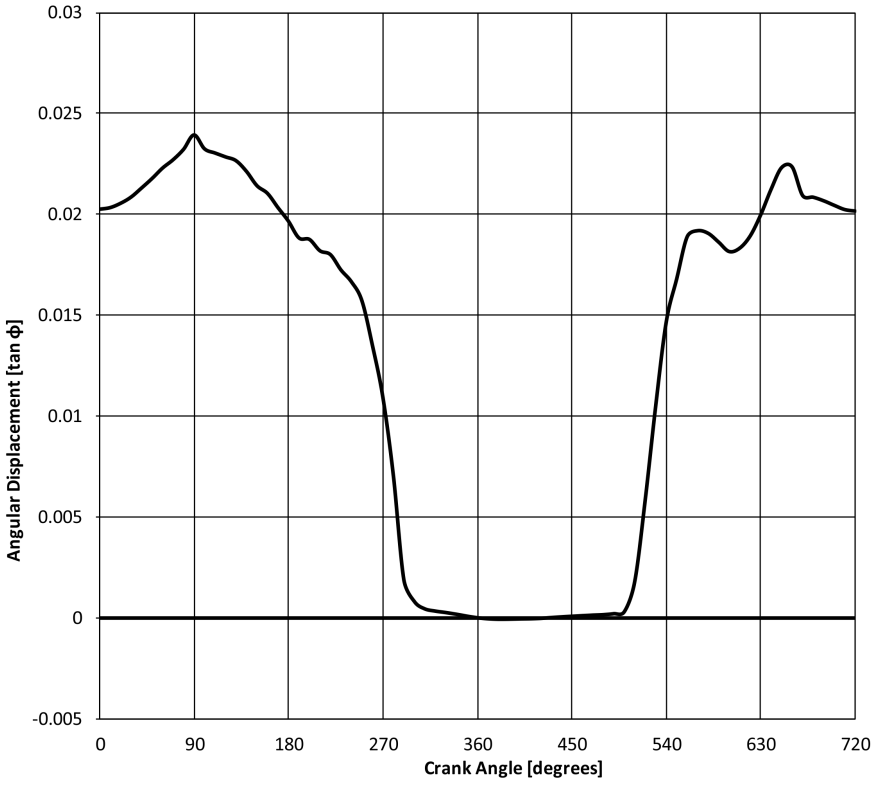

Figure 4.3 Angular Displacement

Ring Back Pressure

Neither Tian nor Noordzij present any data for the ring back pressure of this specific test case. Experimental data cannot be obtained with the experimental apparatus described in [13] because there are no pressure transducers placed in this region. In order to approximate the value of the ring back pressure at each time step, a graph of the top ring's upper flank mass flow has been utilized. It has been assumed that the entire mass flow is due to the Poisueille flow described by eq. 4.1, and gas displacement has been neglected. When the upper ring flank is in contact with the oil film (no mass flow is present), the back pressure is assumed to be equal to the pressure at the lower region (fig.4.4). This assumption should be correct because the lower flank's Poisueille flow is negligible. When there is no oil film contact (fig.4.5) the back pressure is obtained by solving eq.3.28 for p_b:

$$p_b = \sqrt{p_a^2 - \dot{m}_{gas} 24 \mu_{gas} RT \int_{x_a}^{x_b} \frac{dx}{h_{gas}^3(x)}} \tag{4.1}$$

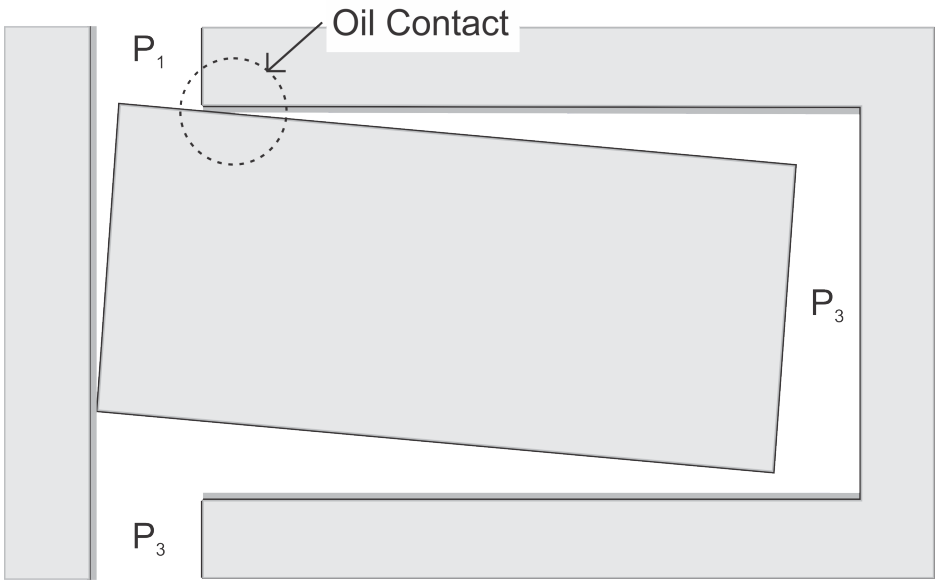

Figure 4.4 Pressures when there is oil contact at the top

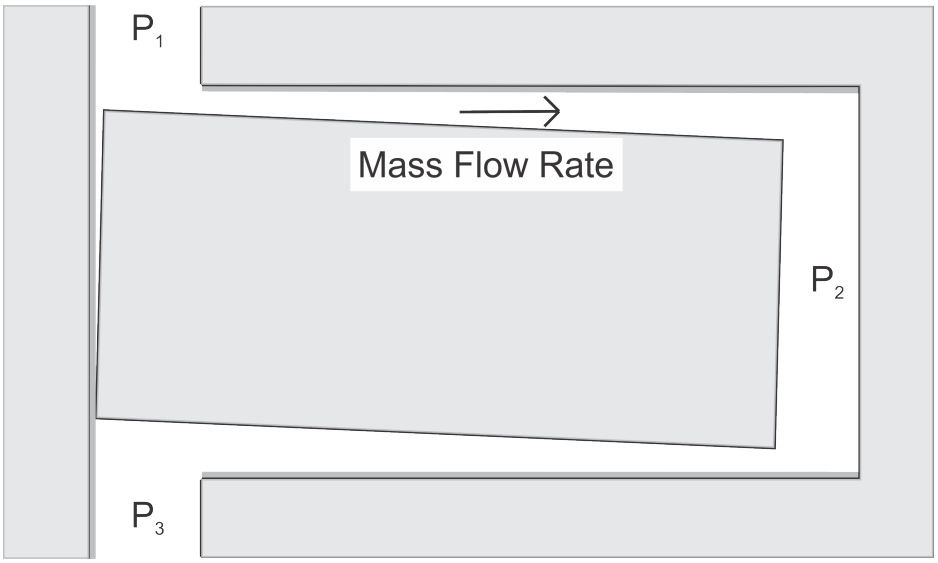

Figure 4.5 Pressures when there is no oil contact at the top

4.2 Results

4.2.1 Ring-Groove Gas Model

The gas mass flow rate is calculated using the Poiseuille's equation for mass flow (eq. 3.28). There should be an exact agreement with Tian's results due to the procedure that has been followed, which is essentially an identity because the same equation that has been solved for the back pressure is now solved for the mass flow rate. The purpose of this comparison is to examine whether the algorithm and the accuracy of the numerical procedure are sufficient. Thus, figure 4.6 below can not be treated as a result and does not prove the validity of the model.

The gas mass flow through the lower flank is zero, as expected, due to the zero pressure difference that has been imposed between the ring back pressure and the lower pressure (fig. 4.5) when there is no oil contact.

The ring gap flow rate should be exact between crank angles $326deg$ and $440deg$, where there were no pressure values presented in Tian's work and a similar procedure with the gas mass flow rate was followed. However the non-linear nozzle flow equation (eq. 2.27) was not solved for the upper pressure, so the iterative procedure that was used may have a slight deviation. As shown in figure 4.7, the agreement is very good between these crank angles. Outside the above region, the upper pressure was measured from a figure and blended with the rest of the values. The calculations in these regions is, unlike the region discussed above,

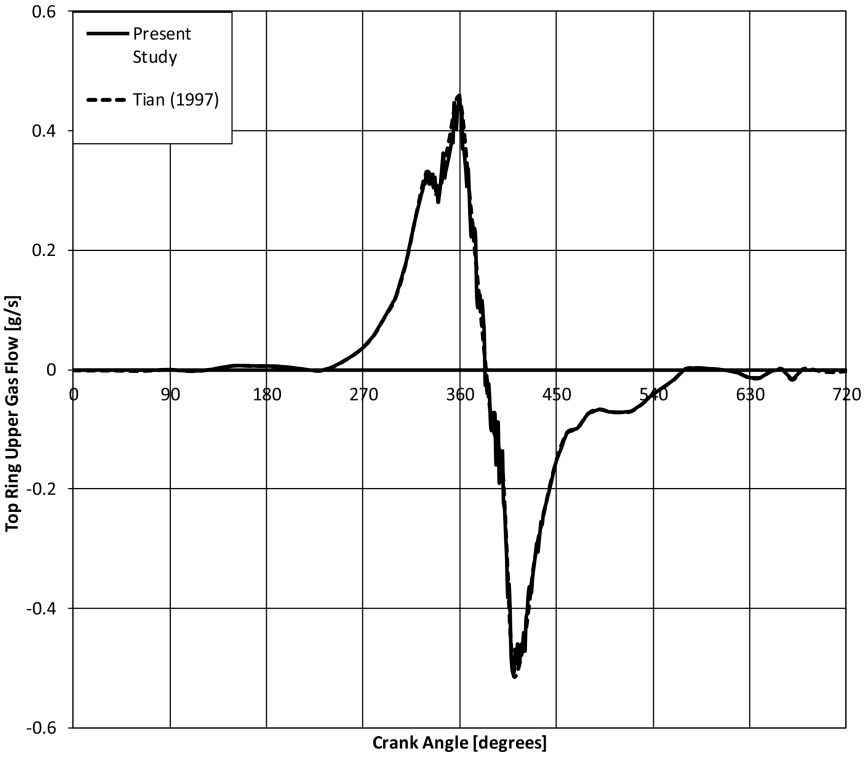

Figure 4.6 Gas mass flow rate through the upper flank of the top ring

a result of the model and should be treated as such. A small deviation is present, which can be attributed to the following reasons:

- Reduced accuracy of the figures providing input data.
- Changes of gap size affect pressure values in the upper ring region. In the experiments of [13], three different cases with three different ring gap sizes were measured, therefore there is a chance that the pressure presented in Tian's study corresponded to a different case.

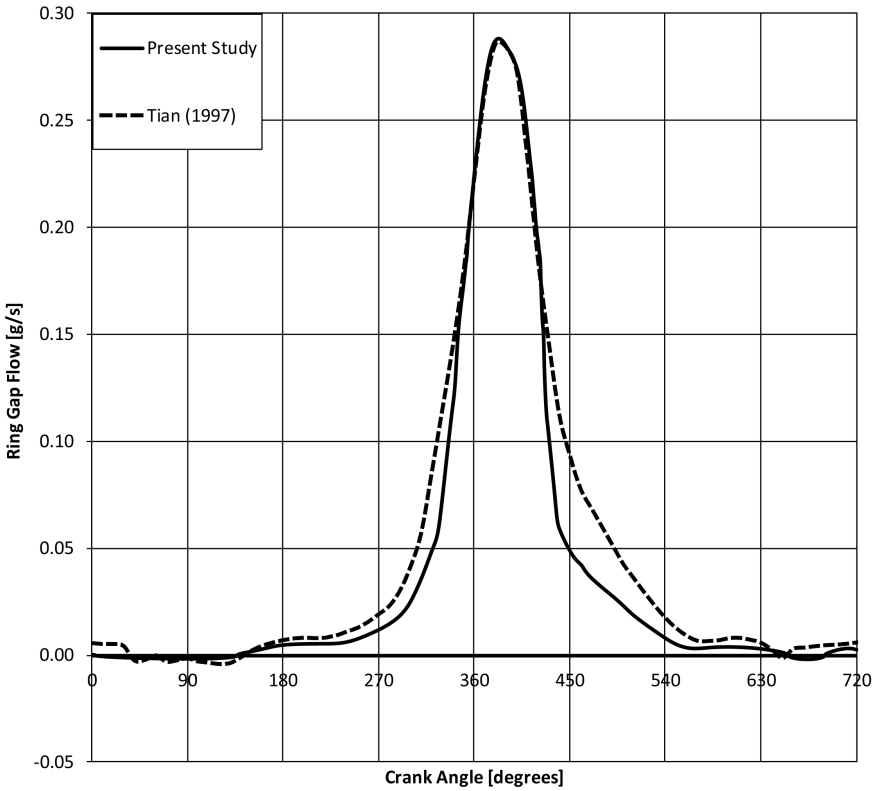

Figure 4.7 Ring gap gas mass flow

Next, the pressure generated by the gas on the upper ring side is presented in comparison with Tian's results in the figure below (fig.4.8). This figure includes the oil force, however, the ring is not in contact with the upper groove side after crank angle $90deg$ and until $680deg$ and, furthermore, in the initial oil contact region, the ring-groove distance is increasing so there is no oil force that is being generated.

The apparent deviation in the graph is attributed to the fact that mass flow in figure 4.6 includes the flow due to gas displacement which is not calculated in the present model (assumed negligible). It is noted that, gas displacement does not generate any pressure, which is

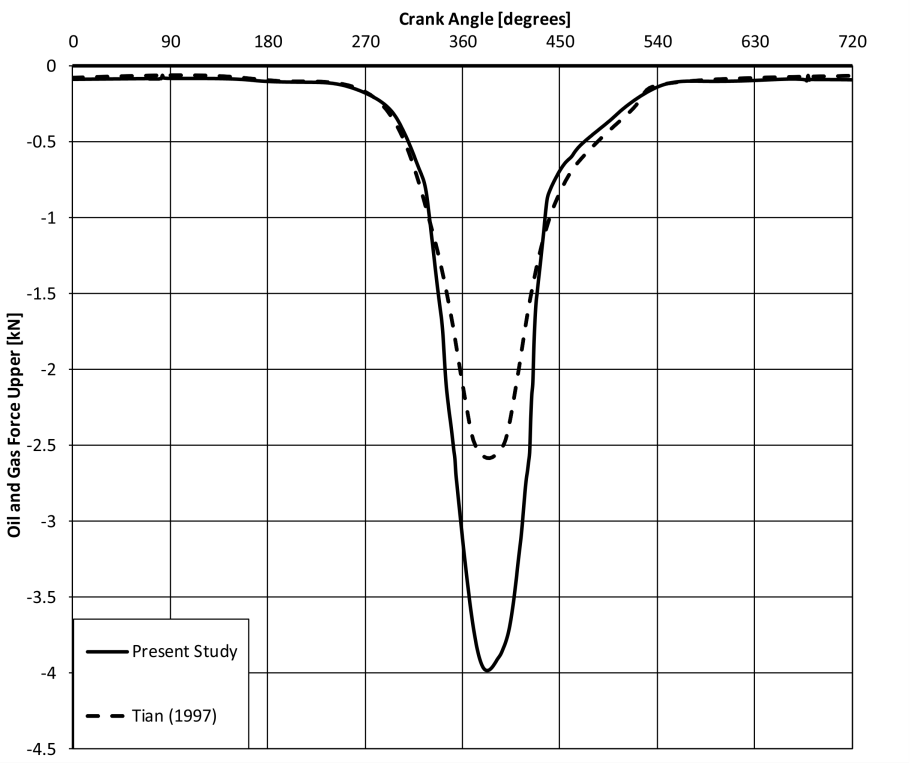

Figure 4.8 Oil and gas force generated in the upper channel

in contrast to the results of the used Poiseuille gas flow, leading to an overestimation of pressure and, thus, force. In equation 3.24, the mass flow due to gas displacement is expressed as a function of the derivative of the pressure with respect to time. In the region of crank angles where deviation occurs (late compression stroke and early power stroke), pressure changes rapidly, therefore mass flow due to gas displacement has values large enough, that should compensate for the deviation observed.

4.2.2 Oil Contact Model

For the oil contact model, the validation is done using the oil and gas force in the lower flank of the groove. The gas force, unlike the case of the upper flank, is small, because there is no gas mass flow due to oil contact and, when no oil contact occurs, there is no pressure difference between the region behind the ring and the lower region.

As expected, the deviation is much smaller and can be attributed to figure reading errors and to the fact that the oil viscosity value (estimated in the present model) may be different from that used in Tian's work.

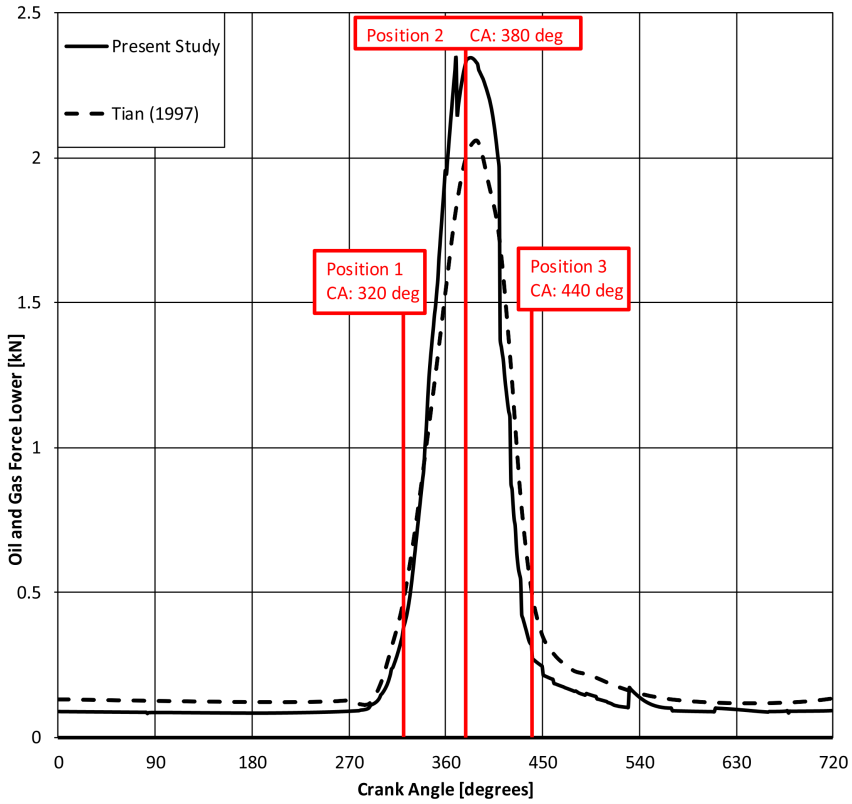

Figure 4.9 Oil and gas force generated in the lower channel

The ring moment generated by the oil force is presented below (fig.4.10). The fact that the moment has negative values means that it tends to rotate the ring in such a way that the outer edge goes down (anticlockwise according to fig.3.1 and the figures in this thesis in general)

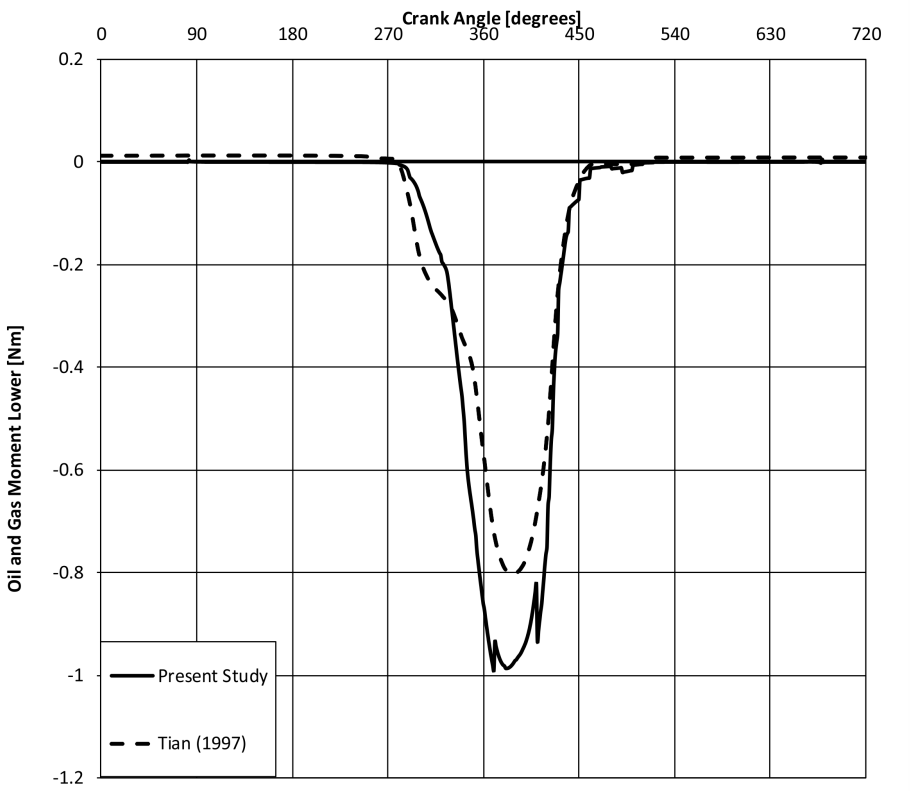

Figure 4.10 Oil and gas moment generated in the lower channel

In figure 4.9 three different positions are noted: CA:320, 380, 440 deg. At these positions, figures 4.11-4.13 depict the oil pressure distribution generated in the lower channel along with the distance between the lower flank of the ring and the lower flank of the groove. The secondary axis (on the right) has a maximum value of $2\mu m$ which is equal to the oil film thickness. This way the ring flank is shown only when it is in the oil region. In the figures 4.11 and 4.13 it is shown how the angular and axial velocity becomes important for the oil pressure generation. Even if the ring flank is within the oil region, the oil does not generate force unless the ring is approaching the groove at a given position. In further detail, fig. 4.11 it is depicted that the oil is not generating any pressure between positions $-1.0r_d/2$ and up until around $-0.75r_d/2$, because, although the centre of the flank is approaching the groove surface, the rotational speed together with the axial speed result in an overall upwards motion of the region. An analogous occasion is presented in fig. 4.13 where, although the centre of

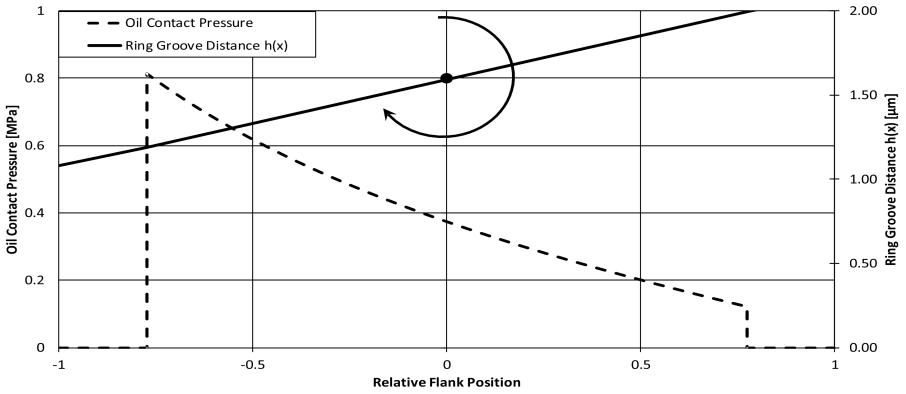

Figure 4.11 Oil pressure distribution generated in the lower channel at CA:320 deg

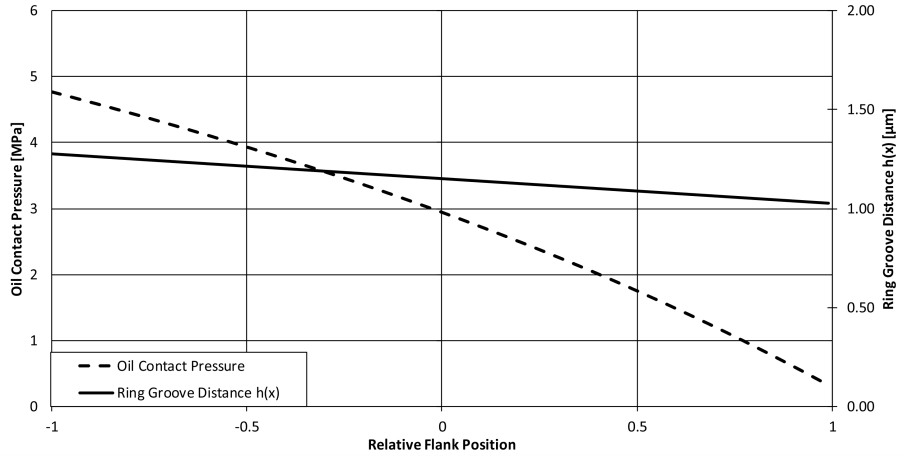

Figure 4.12 Oil pressure distribution generated in the lower channel at CA:380 deg

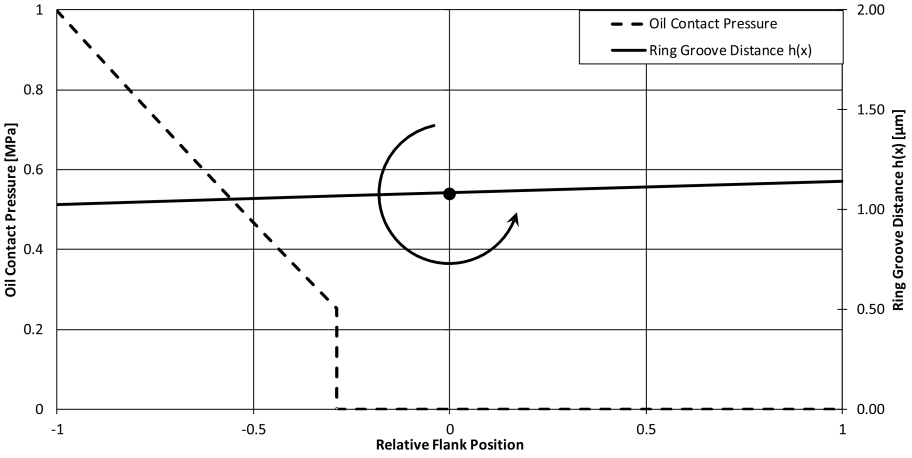

Figure 4.13 Oil pressure distribution generated in the lower channel at CA:440 deg

the ring flank is moving away from the groove, the overall motion of the flank given the rotational speed (illustrated with the arrow) results in an approaching region and, consequently, pressure is being generated between positions $-1.0r_d/2$ and approximately $-0.3r_d/2$.

4.2.3 Asperity Contact Model

The asperity contact is generated when the ring-groove distance becomes smaller than the critical value of 4σ where σ is the variance of the composite surface roughness. The graphs that can be used for validation are an asperity contact force graph and an asperity contact moment graph presented in Tian's work [18]. In the graphs below (fig. 4.14 and fig. 4.15) the asperity contact force and moment, respectively, that were calculated in the present study are presented.

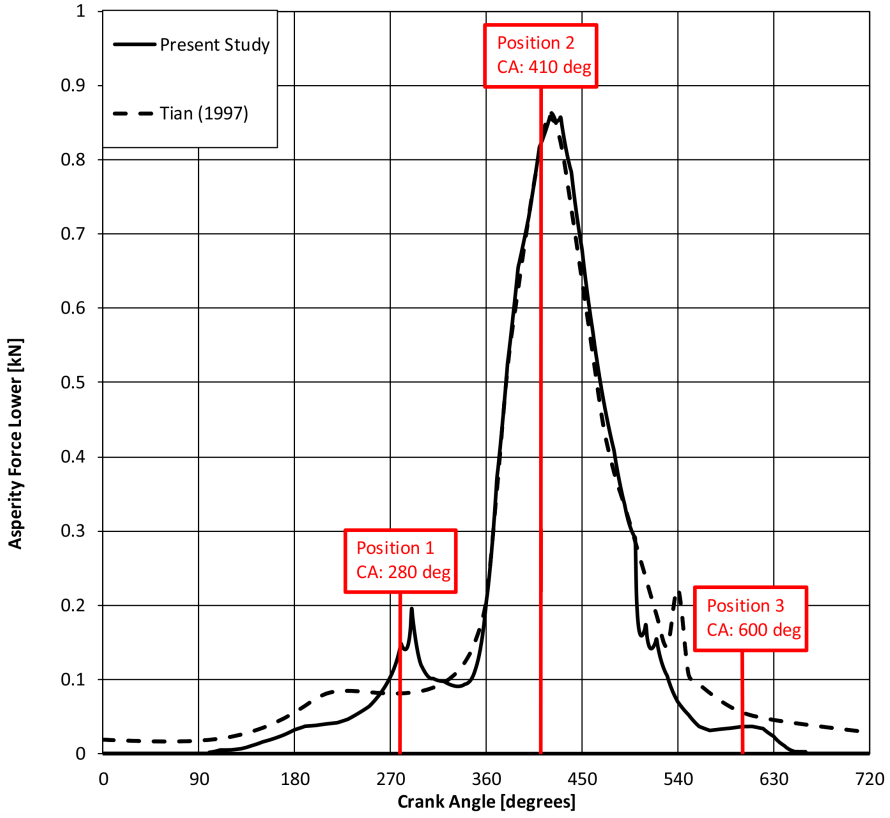

Figure 4.14 Asperity contact force generated in the lower channel

Any deviation between the calculated force and moment in the present study and that of Tian can be attributed to the following factors:

- The force and moment from the asperity contact are very sensitive to the motion and the position of the ring.

- Even though the ring motion was described by combining data from 4 different graphs from [18], the accuracy of the figures may have been reduced.
- There is no direct information regarding the centre of rotation of the ring, so a slight deviation between the centre that has been assumed in the present study and that in Tian's work might be different. That can affect the force and moment values.
- There is no information regarding the parameters K', A and z used in Tian's work. These parameters were assumed to be similar to what was used by Hu et al. in [7]. Furthermore, the combined elastic modulus was calculated by the Young's moduli presented in table 4.1 which are also assumed and are not provided by Tian.

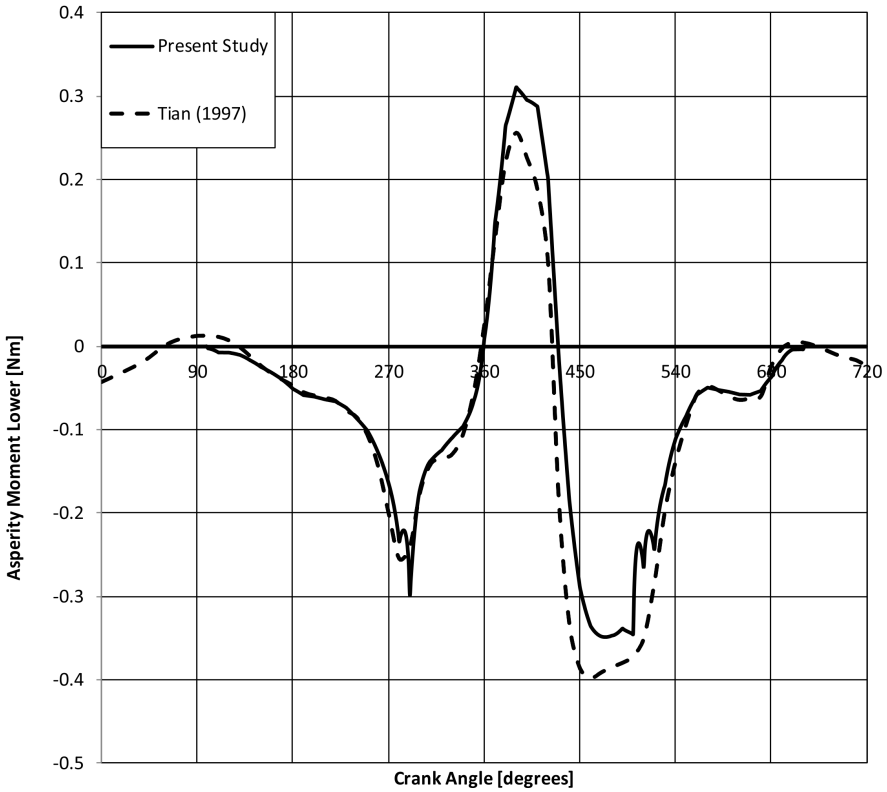

Figure 4.15 Asperity contact moment generated in the lower channel

In figure 4.14 three different positions are noted. In these positions, the corresponding figures 4.16-4.18 present the asperity contact pressure distribution along the lower ring flank, the size of which is dictated by eq. 2.39. In contrast to the oil contact, the asperity pressure is related only to the distance between the ring flank and the groove and not to the velocity of the ring flank. The ring flank is also presented in the figures and the values are indicated on the secondary (right) axis. The maximum value of the secondary axis is equal to $4\sigma = 2\mu$

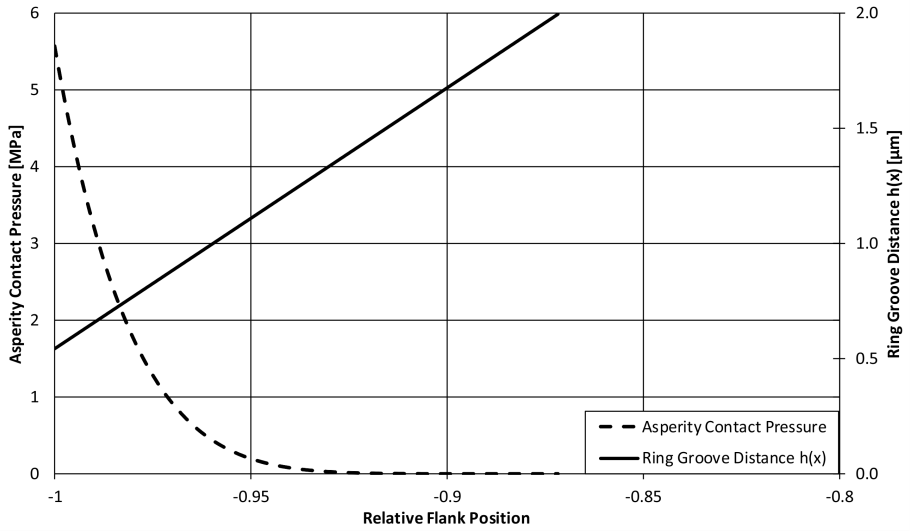

Figure 4.16 Asperity contact distribution generated in the lower channel at CA:280 deg

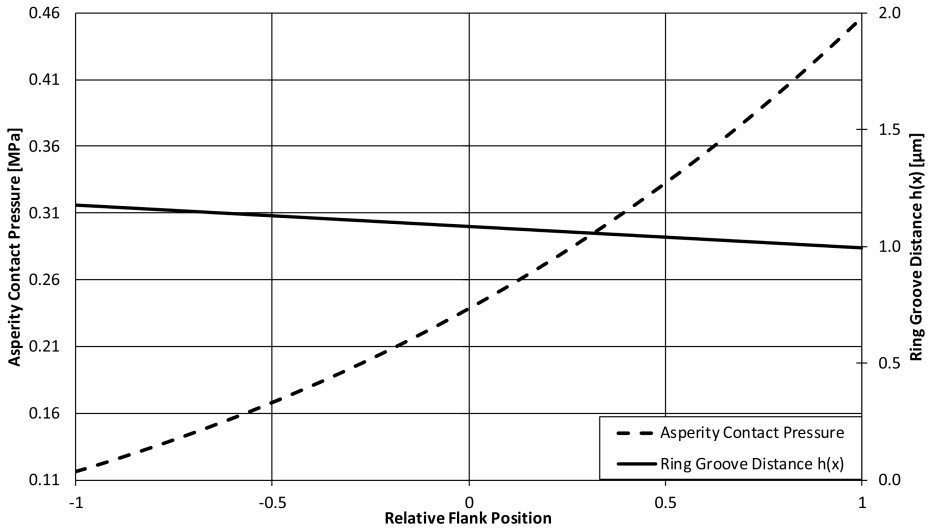

Figure 4.17 Asperity contact distribution generated in the lower channel at CA:410 deg

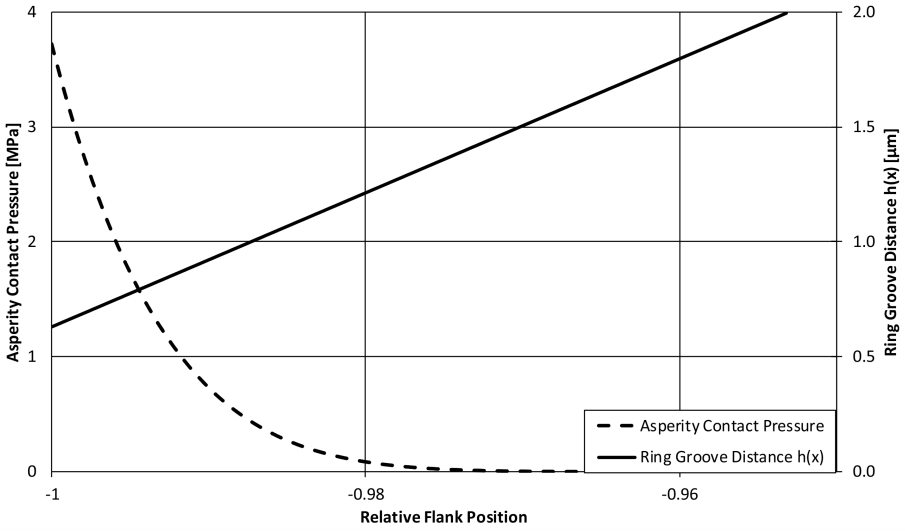

Figure 4.18 Asperity contact distribution generated in the lower channel at CA:600 deg

which is the critical value under which asperity contact pressure is generated. Specifically, in figures 4.16 and 4.18 only a part of the ring flank is in the asperity contact area and the distribution generates a moment that tends to move the ring in a anti-clockwise direction (negative moment) according to fig.3.1. This can also be seen in fig.4.15 at the corresponding crank angle positions. It is important to be noted that the negative axis in the lower flank starts at the inner edge, as opposed the the upper flank and the way that the plot figures are presented. In figure 4.17 it is apparent that the pressure distribution is generated on the entire flank and has lower values that the prior occasions due to larger clearances. The distribution generates a clockwise (positive) moment which is also compatible with the presented curve in fig.4.15.

Chapter 5

Summary

5.1 Conclusions

In this study an two-dimensional model that is capable of calculation of coupled ring and gas dynamics in internal combustion engines has been presented. First, a physical analysis has been performed in order to model and formulate the forces and moments acting on the rings, as well as the gas flows occurring in the various channels in the ring pack system. Next, numerical formulation of the physical model has been performed in order to enable software implementation. In addition, a case study was carried out, simplifying the described model above. The simplified model algorithm received as input the various parameters of a test case, together with ring motion data (axial and angular displacement as a function of the crank angle). The algorithm was able to yield the pressure distribution along the ring flank, along with the force and moment, generated by three different mechanisms:

- Gas pressure
- Oil film squeezing
- Asperity contact

Furthermore, gas mass flow rates through the ring groove channels and ring gap were calculated. An overall sufficient agreement with the results provided in [18] and [13] has been observed.

Various figures were generated, illustrating each different output of the algorithm in a comprehensive manner, and providing an intuitive depiction of the physical interaction between the ring and the groove. Moreover, comparative figures with both the results of the present study and the results of Tian [18] were plotted. The output data and figures were then reviewed and any occurring deviations and discrepancies were evaluated and discussed.

5.2 Future Work

The model described in the framework of the present thesis can be used for corresponding software development, although many numerical instabilities might be present, as it was indicated by attempts made by the author.

Coupling of the present model that describes ring and gas dynamics with a ring-liner interaction model should provide important results (for example as shown in fig. 1.1). Such a model would be able to accurately predict blowby and ring-liner friction losses. Consequently, the combined model would be eligible to be used for parametric studies or multi-objective optimization studies.

On another path, the present study indicated that it is able to predict pressure distribution on the ring. Thus, it would be possible for this model to be combined with wear theory for the development of an integrated solution, capable of estimating wear according to various design parameters.

Bibliography

[1] Andersson, P., Tamminen, J., and Sandström, C.-E. (2002). Piston ring tribology. *A literature survey. VTT Tiedotteita-Research Notes*, 2178(1).

[2] Cho, S.-H., Ahn, S.-T., and Kim, Y.-H. (2002). A simple model to estimate the impact force induced by piston slap. *Journal of Sound and vibration*, 255(2):229–242.

[3] Chong, W. W. F., Teodorescu, M., and Vaughan, N. D. (2011). Cavitation induced starvation for piston-ring/liner tribological conjunction. *Tribology International*, 44(4):483–497.

[4] Dowson, D. (1993). Piston assemblies; background and lubrication analysis. *Tribology Series*, 26:213–240.

[5] Ellerman, A. D. and Joskow, P. L. (2008). *The European Union's emissions trading system in perspective*. Pew Center on Global Climate Change Arlington, VA.

[6] Greenwood, J. and Tripp, J. (1970). The contact of two nominally flat rough surfaces. *Proceedings of the institution of mechanical engineers*, 185(1):625–633.

[7] Hu, Y., Cheng, H. S., Arai, T., Kobayashi, Y., and Aoyama, S. (1994). Numerical simulation of piston ring in mixed lubrication—a nonaxisymmetrical analysis. *Journal of tribology*, 116(3):470–478.

[8] Jeng, Y.-R. (1992). Theoretical analysis of piston-ring lubrication part i—fully flooded lubrication. *Tribology Transactions*, 35(4):696–706.

[9] Keribar, R., Dursunkaya, Z., and Flemming, M. F. (1991). An integrated model of ring pack performance. *ASME, Transactions, Journal of Engineering for Gas Turbines and Power*, 113:382–389.

[10] Koukoulopoulos, E. (2014). Software development for the solution of hydrodynamic lubrication problems in piston rings of two-stroke marine diesel engines.

[11] Liu, L. (2005). *Modeling the performance of the piston ring-pack with consideration of non-axisymmetric characteristics of the power cylinder system in internal combustion engines*. PhD thesis, Massachusetts Institute of Technology.

[12] Namazian, M. and Heywood, J. B. (1982). Flow in the piston-cylinder-ring crevices of a spark-ignition engine: effect on hydrocarbon emissions, efficiency and power. Technical report, SAE Technical Paper.

[13] Noordzij, L. B. (1996). *Measurement and analysis of piston inter-ring pressures and oil film thickness and their effects on engine oil consumption*. PhD thesis, Massachusetts Institute of Technology.

[14] Psaraftis, H. N. and Kontovas, C. A. (2010). Balancing the economic and environmental performance of maritime transportation. *Transportation Research Part D: Transport and Environment*, 15(8):458–462.

[15] Rabute, R. and Tian, T. (2001). Challenges involved in piston top ring designs for modern si engines. *TRANSACTIONS-AMERICAN SOCIETY OF MECHANICAL ENGINEERS JOURNAL OF ENGINEERING FOR GAS TURBINES AND POWER*, 123(2):448–459.

[16] Richardson, D. E. (2000). Review of power cylinder friction for diesel engines. *TRANSACTIONS-AMERICAN SOCIETY OF MECHANICAL ENGINEERS JOURNAL OF ENGINEERING FOR GAS TURBINES AND POWER*, 122(4):506–519.

[17] Shapiro, A. H. (1953). *The dynamics and thermodynamics of compressible fluid flow*. John Wiley & Sons.

[18] Tian, T. (1997). *Modeling the performance of the piston ring-pack in internal combustion engines*. PhD thesis, Massachusetts Institute of Technology.

[19] Tian, T., Noordzij, L., Wong, V., and Heywood, J. (1998). Modeling piston-ring dynamics, blowby, and ring-twist effects. *Journal of engineering for gas turbines and power*, 120(4):843–854.

[20] Ting, L. and Mayer, J. (1974). Piston ring lubrication and cylinder bore wear analyses, part ii—theory verification. *Journal of lubrication technology*, 96(2):258–266.

[21] Ting, L. and Mayer Jr, J. (1974). Piston ring lubrication anl cylinder bore wear analysis, part i—theory1. *Journal of Lubrication Technology JULY*, page 305.

[22] Zhao, J. X. and Chia-fon, F. L. (2006). Modeling of blow-by in a small-bore high-speed direct-injection optically accessible diesel engine. Technical report, SAE Technical Paper.

[23] Zhu, D., Cheng, H. S., Arai, T., and Hamai, K. (1992). A numerical analysis for piston skirts in mixed lubrication—part i: Basic modeling. *Journal of tribology*, 114(3):553–562.